Global and Planetary Change 169 (2018) 1–15

Contents lists available at ScienceDirect

Global and Planetary Change

journal homepage: www.elsevier.com/locate/gloplacha

Reasearh Article

New $^{40}Ar/^{39}Ar$, magnetostratigraphic and biostratigraphic constraints on the termination of the Badenian Salinity Crisis: Indications for tectonic improvement of basin interconnectivity in Southern Europe

A. de Leeuw[a,b,g,*], M. Tulbure[c,d], K.F. Kuiper[e], M.C. Melinte-Dobrinescu[f], M. Stoica[c], W. Krijgsman[a]

[a] Paleomagnetic Laboratory 'Fort Hoofddijk', Faculty of Geosciences, Utrecht University, Budapestlaan 17, Utrecht CD-3584, The Netherlands
[b] CASP, West Building, 181a Huntingdon Road, Cambridge CB3 0DH, United Kingdom
[c] Department of Geology, Faculty of Geology and Geophysics, University of Bucharest, Bălcescu Bd. 1, 010041, Romania
[d] Department of Earth Sciences, University of Utrecht, Budapestlaan 4, Utrecht, The Netherlands
[e] Faculty of Earth and Life Sciences, Department of Earth Sciences, Vrije Universiteit Amsterdam, De Boelelaan 1085, Amsterdam 1081 HV, The Netherlands
[f] National Institute of Marine Geology and Geo-Ecology (GEOECOMAR), 23-25 Dimitrie Onciul Street, Bucharest RO-024053, Romania
[g] Univ. Grenoble Alpes, Univ. Savoie Mont Blanc, CNRS, IRD, IFSTTAR, ISTerre, 38000 Grenoble, France

ARTICLE INFO

Keywords:
Paleo-environment
Marine gateways
Geochronology
Stratigraphy
Paratethys

ABSTRACT

Widespread evaporites were deposited in large parts of the Central Paratethys during the so-called Badenian Salinity Crisis (BSC). The adverse environmental conditions that accompanied the BSC triggered a demise in the basin's marine fauna, inducing the so-called middle-Badenian-extinction-event. While tectonic activity preconditioned the Central Paratethys for isolation, it has recently been shown that the BSC was eventually triggered by the base-level drop accompanying the Mi3b global cooling event, which terminated the Middle Miocene Climatic Optimum. Here, we provide new constraints on the termination of the BSC by $^{40}Ar/^{39}Ar$ dating of a volcanic ash layer, located in a marl succession several meters above the Badenian evaporites of the Slănic Syncline in the Romanian East Carpathians. The results reveal that the BSC ended before 13.32 ± 0.07 Ma. Comparison with previously obtained geochronological results in Poland constrains the duration of the BSC to 500 kyr, assuming evaporite deposition in the Central Paratethys occurred as one event. The obtained $^{40}Ar/^{39}Ar$ results are complemented with paleomagnetic and micropaleontological analyses. These reveal that the investigated post-BSC marl interval in the Slănic Syncline was deposited in a period of reversed polarity corresponding to C5AAr. This is in agreement with calcareous nannoplankton from the same interval that belong to the NN6 zone. Ostracod and foraminifera marker species are indicative of the middle part of the regional Badenian stage, traditionally known as the Wielician. The foraminiferal assemblage is nevertheless very similar to Serravallian assemblages from the Mediterranean, which suggests that, in addition to a connection between the Central Paratethys and the Eastern Paratethys, there was a marine connection with the Mediterranean following the BSC. A comparison with post-BSC successions in Ukraine and Poland illustrates that the BSC was terminated by a transgression that re-installed normal marine conditions in the Carpathian foredeep. This basin-wide transgression resulted from reconnection of the Carpathian Foreland Basin with the Mediterranean and Eastern Paratethys, which improved the exchange of water and fauna. Global eustacy cannot explain re-connection of these basins, because global sea level on average remained just as low after the BSC as it had been during the crisis. The improved interconnectivity between the basins must therefore have been primarily caused by tectonic modification of the interconnecting gateways. Geodynamics thus played a crucial role in the re-establishment of a flourishing marine environment.

1. Introduction

Semi-enclosed basins like the Paratethys and Mediterranean are exceptionally suitable to study the forcing mechanisms of (paleo-)environmental change. The land-locked Paratethys was mainly connected to the open ocean via shallow and narrow marine gateways (Steininger

* Corresponding author at: Univ. Grenoble Alpes, Univ. Savoie Mont Blanc, CNRS, IRD, IFSTTAR, ISTerre, 38000 Grenoble, France.
E-mail addresses: arjan.deleeuw@casp.cam.ac.uk, arjan.de-leeuw@univ-grenoble-alpes.fr (A. de Leeuw).

https://doi.org/10.1016/j.gloplacha.2018.07.001
Received 27 February 2017; Received in revised form 4 July 2018; Accepted 4 July 2018
Available online 06 July 2018
0921-8181/

and Rögl, 1984; Rögl, 1998; Popov et al., 2004). Hydrological changes due to restriction or expansion of these gateways had a marked impact on the paleoenvironmental conditions in the Paratethys basins (e.g. Karami et al., 2011; Palcu et al., 2015) and contributed to a number of extinction events (Harzhauser and Piller, 2007). The most extreme environmental changes are so-called salinity crises that occur when marine connections are progressively closed resulting in restriction, isolation and massive salt deposition (Krijgsman et al., 2000; Peryt, 2006; Roveri et al., 2014; CIESM, 2008). The Miocene Badenian stage of the regional Paratethys time scale is marked by major paleoclimatic fluctuations and increased geodynamic activity that, combined with deteriorated water circulation patterns, resulted in hypersaline conditions in large parts of the Central Paratethys (Kováč et al., 2007). During this so-called Badenian Salinity Crisis (BSC), formation of widespread salt and gypsum deposits took place in the Carpathian Foredeep, Transylvanian, Transcarpathian and East-Slovak basins (Venglinskij, 1975; Kováč et al., 1995, 1996; Filipescu, 2001; Krézsek and Filipescu, 2005; Peryt, 2006). Recently discovered Badenian salt deposits along the Mid-Hungarian shear zone (Palotai and Csontos, 2012; Báldi et al., 2017) and stromatolitic deposits in the Austrian Oberpullendorf Basin that are indicative of hostile hypersaline conditions (Harzhauser et al., 2014) reveal that the BSC possibly also had a strong environmental impact on the Pannonian Basin. The BSC went hand in hand with a significant demise in the basins gastropod and ostracod fauna, which has been coined the middle-Badenian-extinction-event (Harzhauser and Piller, 2007).

A reliable chronologic framework is crucial to unravel climatic from geodynamic forcing factors on evaporite formation (Hodell et al., 2001; Krijgsman et al., 2004). Radio-isotope dating recently indicated that, following tectonic preconditioning of the Central Paratethys for isolation, the onset of the BSC was eventually triggered by the Mi3b global cooling event which terminated the Middle Miocene Climatic Optimum (de Leeuw et al., 2010). This corresponding cooling event is expressed in changes in foraminifera assemblages and stable isotope ratios in the marls directly underlying the evaporites (Bicchi et al., 2003; Gonera et al., 2000; Gonera, 2013; Peryt, 2013b). The corresponding sea level lowering restricted the marine gateways to the Mediterranean, resulting in hypersaline conditions in the Central Paratethys. Based on interpolation of $^{40}Ar/^{39}Ar$ ages, the total duration of Badenian evaporite deposition was estimated to be ~400 ± 200 kyr (de Leeuw et al., 2010). Additional high resolution age constraints on the termination of the BSC are necessary to elucidate the exact forcing mechanisms of salt and gypsum in these marine environments and to establish what caused the end of the BSC.

In this paper, we focus on the termination and duration of the Badenian Salinity Crisis. The end of the BSC will be determined by $^{40}Ar/^{39}Ar$ dating of a volcanic ash layer, located in a marl succession several meters above the Badenian evaporites of the East Carpathians in Romania (Fig. 1). It will be shown that the obtained age statistically overlaps with complementary $^{40}Ar/^{39}Ar$ dates from a volcanic ash in the Pecten Beds that overlie BSC evaporites in Poland (Śliwiński et al., 2012) after recalibration to the astronomically tuned age of the FCs standard. A comparison of these post-BSC ages with the $^{40}Ar/^{39}Ar$ ages from the base and middle of the BSC successions in southern Poland, (de Leeuw et al., 2010; Bukowski et al., 2010), will moreover constrain the duration of the BSC. Biostratigraphic and magnetostratigraphic results from the post-evaporitic marls at Piatra Verde will complement the obtained radio-isotopic age. Detailed faunal analyses on planktonic and benthonic foraminifera, calcareous nannofossils and ostracods will shed light on the paleoenvironmental and paleogeographic changes that re-installed open marine environments in the East Carpathian Foredeep directly after the BSC.

2. Badenian evaporites in the East Carpathians (Romania)

Badenian evaporites of the Central Paratethys are generally 30–100 m thick and consist of gypsum or halite with intercalations of clay. Facies analyses suggest that the Badenian halite originated from deep density-stratified brines (Bąbel, 1999) and slightly pre-dated the onset of gypsum at the basin margins (Peryt, 2006). Badenian strata in the eastern part of the Central Paratethys, including the Carpathian Foreland Basin, have a three-partite division (Papp et al., 1978; Piller et al., 2007). There is a lower interval with open marine siliciclastics and carbonates, which is overlain by a middle interval with evaporites, which is in turn overlain by an upper interval with open marine siliciclastics. These three intervals can easily be distinguished in the field and on seismic sections and roughly correspond with the Moravian, Wielician and Kosovian biostratigraphic zones, frequently used in the eastern part of the Central Paratethys (Piller et al., 2007). However, the definition and extent of these zones varies and the Wielician extends both below and above the evaporites (Gonera, 2013). There is furthermore an ongoing debate on the subdivision of the Badenian of the Central Paratethys and various substage definitions have been proposed (c.f. Papp et al., 1978; Piller et al., 2007; Kováč et al., 2007; Hohenegger et al., 2014). We do not intend to contribute to, or resolve this discussion, but rather provide radio-isotopic age constraints on a typical BSC succession in Romania. We provide detailed information on the calcareous nannoplankton, ostracod and foraminifer assemblages in the investigated section, which should enable direct comparison with other Badenian successions and alternative subdivisions proposed.

In the Romanian part of the former Carpathian Foredeep, the BSC deposits comprise halite with thin claystone and siltstone intercalations, gypsum and breccias. Massive halite deposits occur in the salt diapir of Slănic-Pahova (Fig. 2). In-situ selenitic saber-like gypsum deposits and microbial stromatolites, which accumulated in shallower salina-type parts of the basin, crop out along Valea Rea, where they superpose tuff-bearing lower Badenian “Globigerina Marls” (Crihan, 1999; Frunzescu, 2005). They are unconformably overlain by a salt breccia which contains clasts of marl, grey-greenish clay, grey fine micaceous calcareous sandstone, gypsum and gypsiferous sandstones, black shales and globigerina-bearing tuffaceous marls (Frunzescu, 2012).

A classical lithostratigraphic succession of the Badenian deposits is exposed at Piatra Verde along the northwest limb of the Slănic Syncline (Fig. 2) (Popescu, 1951; Mărunţeanu, 1999; Melinte-Dobrinescu and Stoica, 2014), which is located in the southernmost East Carpathians. Here, the salt breccia erosively overlies the lower Badenian Slănic Tuff. The latter forms a depositional interval with very prominent volcanic tuffs and tuffites interbedded with “Globigerina Marls” that are in places very rich in foraminifera. The larger part of the Slănic Tuff and the associated Globigerina Marls contain calcareous nannofossil assemblages that are typical for the NN5 zone, while the uppermost part lacks index fossil *Sphenolitus heteromorphus* and thus pertains to the NN6 zone (Melinte-Dobrinescu and Stoica, 2014). The overlying salt breccia has a marly to clayey matrix and contains clasts of calcareous sandstones, grey marly limestones, bituminous carbonatic laminites or bituminous shales, *Lithothamnium* limestones, sandstones, green tuffs derived from the adjacent Slănic Tuff and marls with globigeriniids (Frunzescu, 2012). The overlying interval with BSC gypsum is 40–50 m thick and dominated by allochthonous gypsum brought in by debris flows from nearby shallow water salinas (Frunzescu, 2010). The lower part consists of gypsum gravity flow deposits with intermittent layered algal mats. The upper part, which is currently best exposed in the Piatra Verde Hill (Fig. 1; 45°15′32.14″N, 25°58′2.93″E), has a layered alternation of algal- and clastic gypsum deposits at its base, overlain by a 20 m interval of gypsum debris (Frunzescu, 2012). Within the gypsum sequence, there are some very thin silty clay beds that yielded a few molluscs of the *Pycnodonta*, *Ostrea*, *Glycimeris*, *Chlamys*, *Diloma*, *Callistoma* and *Vermetus* genera (Popescu, 1951). There are ~15 m of marls with some intercalating volcanic tuffs on top of the gypsum (Fig. 1c). The overlying upper Badenian of the Slănic Syncline is up to 500 m thick and consists in stratigraphic order of the “Radiolarian Shales”

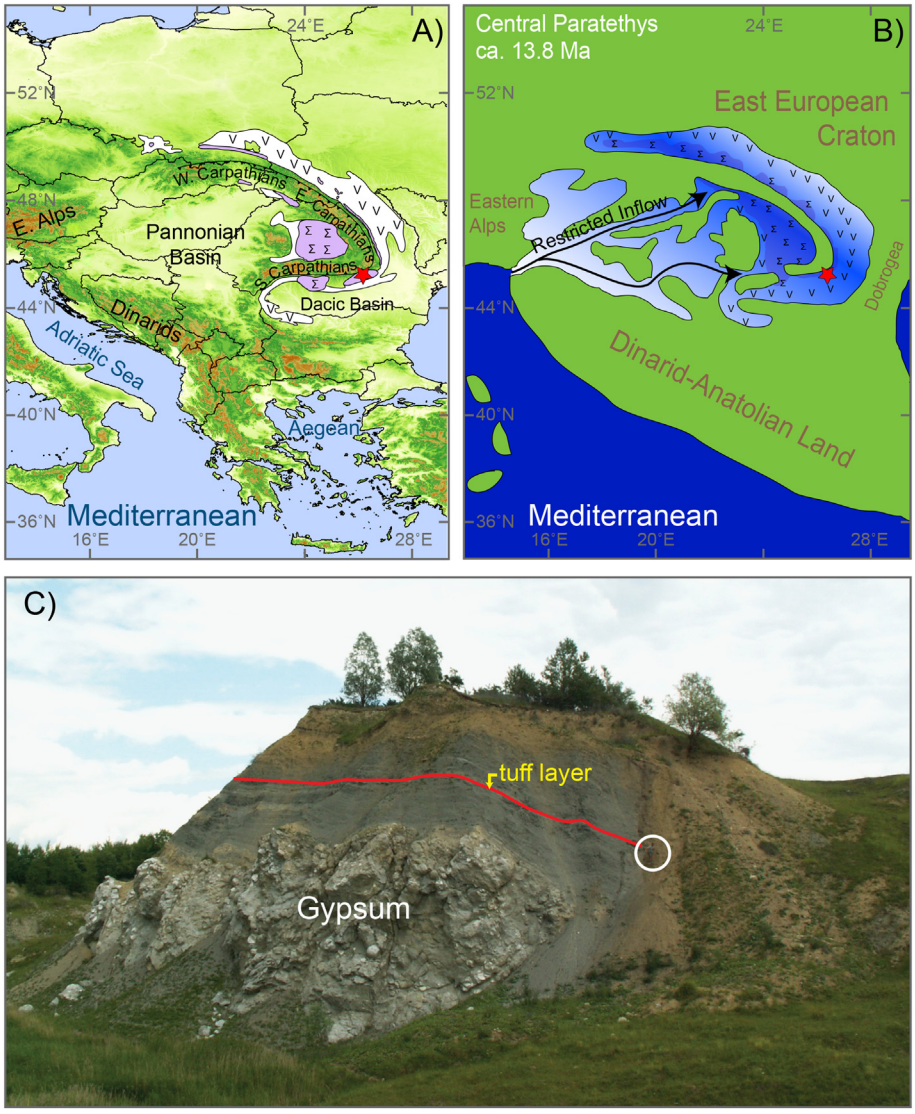

Fig. 1. a) Facies map displaying the distribution of halite (Σ) and gypsum/anhydrite (V) deposits along the Carpathians. Areas with both halite and gypsum/anhydrite are shown as halite. b) Simplified paleogeographic reconstruction of Mediterranean-Paratethys connection during Badenian Salinity Crisis interval (both modified after de Leeuw et al., 2010). Star marks location of studied section. c) Photograph of the Piatra Verde section with the position of the volcanic ash layer. White circle indicates a person for scale.

(argillaceous shales, rich in radiolarians of the *Coenosphaera, Dictyocoryne, Halicapsa, Rhopalodictyum, Sethocapsa* and *Spongodiscus* genera) and "Spirialis Marls" (marls of lutitic facies, locally rich in micro-gastropods) (Popescu, 1951; Motaş et al., 1966; Dumitrică, 1978).

3. Radioisotope dating

We sampled a volcanic ash layer (PV-A) that is located in the marls, ~6 m above the top of the BSC evaporites at Piatra Verde (Fig. 1). The bulk samples were crushed, disintegrated in a dilute calgon solution, washed and sieved over a set of sieves between 63 and 250 μm. The 250–400 μm mineral fraction was subjected to standard heavy liquid and magnetic separation techniques. Biotite separates were submerged in pure demineralized water in an ultrasonic bath for 5 min. Samples were subsequently handpicked and loaded in a 10 mm ID quartz vial together with Fish Canyon Tuff (FC-2) and Drachenfels (Dra-1, f250–500 and Dra-2, f > 500) sanidine serving as flux monitors. The vial was irradiated in the Oregon State University TRIGA reactor in the cadmium shielded CLICIT facility for 10 h.

The separates were then split in two duplicate multigrain fractions that were each loaded in 6 mm holes of a Cu-tray and pre-heated to ~200 °C under vacuum using a heating stage and a heat lamp to remove undesirable atmospheric argon. The tray was then placed in the sample house and the system (extraction line + sample house) was degassed overnight at ~150 °C. Incremental heating was performed with a Synrad CO_2 laser in combination with a Raylase scanhead as a beam delivery and beam diffuser system. After purification the resulting gas was analyzed with a Mass Analyzer Products LTD 215–50 noble gas mass spectrometer. Beam intensities were measured in a peak-jumping mode in 0.5 mass intervals over the mass range 40–35.5 on a Balzers 217 secondary electron multiplier. System blanks were measured every three to four steps. Mass discrimination was monitored by frequent analysis (~every 10 h) of aliquots of air. The irradiation parameter J for each unknown was determined by interpolation between the individually measured standards. $^{40}Ar/^{39}Ar$ ages were calculated with the ArArCalc software (Koppers, 2002). We use the FCs age of 28.201 ± 0.046 Ma (Kuiper et al., 2008) in combination with the decay constants of Steiger and Jäger (1977) for calibration. We are aware that the 28.201 Ma should be used in combination with Min et al. (2000) decay constants, but want to compare this study directly with

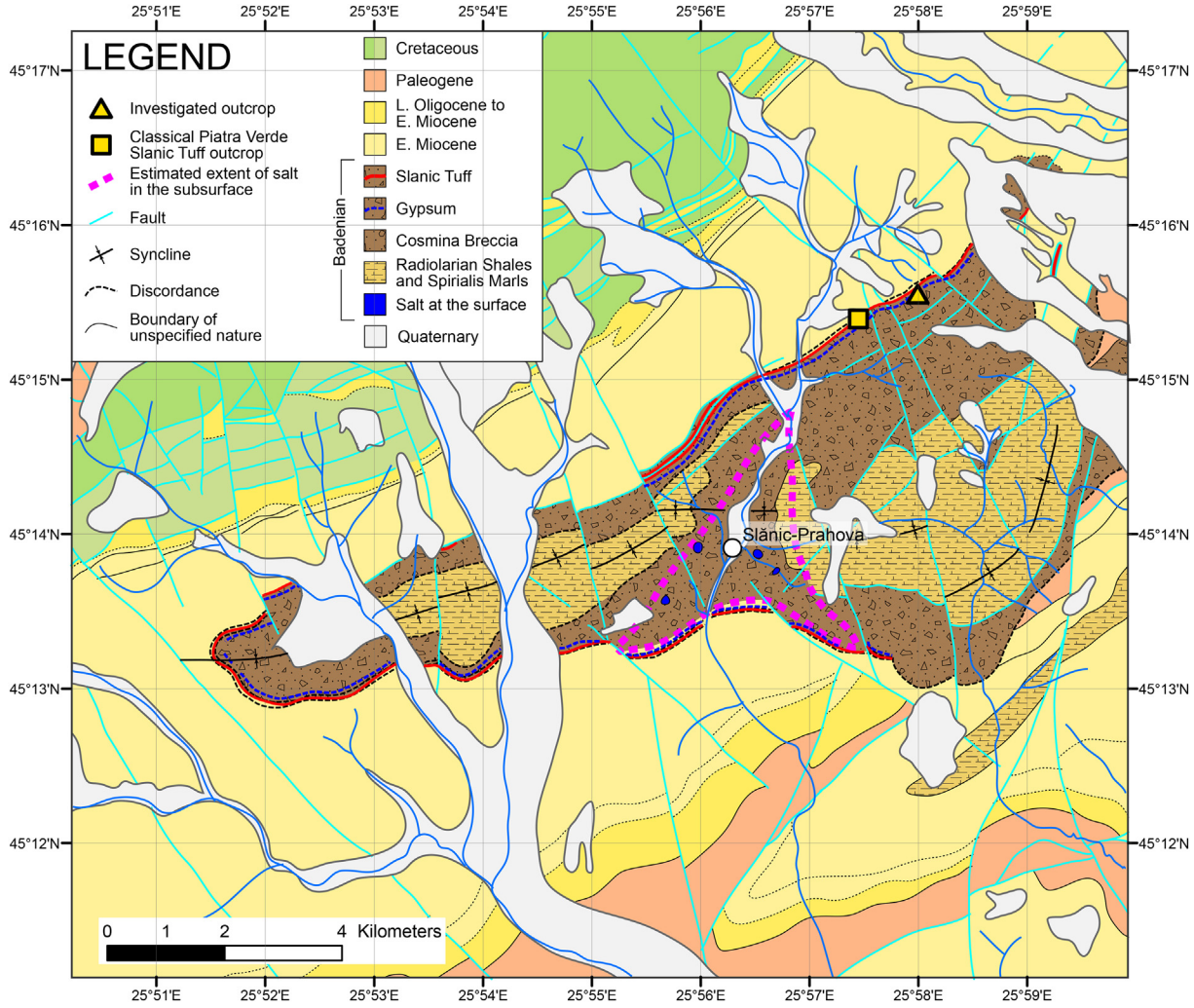

Fig. 2. Geological map of the Slănic Syncline adapted from (Ștefănescu et al., 1978). The syncline is located towards the southern end of the Tarcău Nappe, the most areal widespread tectonic unit of the Moldavide Nappes of the outer East Carpathians (Săndulescu, 1984).

previous results that have been calculated using this calibration model (Bukowski et al., 2010; de Leeuw et al., 2010). If the 28.198 Ma age for FCs based on the Steiger and Jäger decay constants is used, resulting age differences are minor. We report R values (Supplementary Material), so that ages be can recalculated to any preferred calibration model. The age attributed to Drachenfels sanidine that was used as a flux monitor is 25.42 ± 0.03 Ma relative to the FCs age given above. Correction factors for neutron interference reactions are $2.64 \pm 0.017 \times 10^{-4}$ for $(^{36}Ar/^{37}Ar)_{Ca}$, $6.73 \pm 0.037 \times 10^{-4}$ for $(^{39}Ar/^{37}Ar)_{Ca}$, $1.211 \pm 0.003 \times 10^{-2}$ for $(^{38}Ar/^{39}Ar)_{K}$ and $8.6 \pm 0.7 \times 10^{-4}$ for $(^{40}Ar/^{39}Ar)_{K}$. We used the value of 295.5 for the $^{40}Ar/^{36}Ar$ atmospheric ratio (Nier, 1950). Errors are quoted at the 1σ level and include the analytical error and the error in J.

The biotite crystals of the Piatra Verde PV-A ash were irradiated in the same vial and facility as the WT-1 and WT-3 biotite and hornblende samples used to determine the onset of the BSC (de Leeuw et al., 2010). Argon analyses for all these BSC samples were performed using identical analytical protocols and instruments during the same period. In addition we are using the same ages for the Drachenfels and Fish Canyon Tuff flux monitors and the same decay constant. This facilitates direct comparison of the obtained ages.

Standard incremental heating techniques on two duplicate biotite separates (experiments 232 and 233) were performed. The results are summarized in Figs. 3, 4 and Table 1. At low laser power, there is a peak in $^{36}Ar(a)$, while there are low proportions of the other isotopes of argon. This is interpreted to reflect air argon being expelled from "easy" sites in the biotite crystals. This is also reflected in the proportion of 40Ar(r) released, which initially remains very low. At intermediate laser power, the proportion of $^{36}Ar(a)$ released decreases, while there is a strong increase in the proportion of $^{40}Ar(r)$ and $^{39}Ar(k)$. This is taken to reflect the release of radiogenic and potassium generated isotopes of argon during fusion of the biotite crystals. The relatively high K/Ca ratio corroborates fusion of biotite, which generally has 7–8% of potassium content (McDougall and Harrison, 1999), but does not contain calcium. The release of $^{38}Ar(cl)$ is attributed to fusion of some chlorite present in the biotite crystal structure. At high laser power, there is a marked peak in $^{37}Ar(ca)$ and therefore lower K/Ca ratios, while the proportion of radiogenic and potassium generated argon isotopes decreases. This is taken to reflect a diminishing contribution from biotite, while degassing of another, more calcium rich mineral starts to dominate the argon spectrum. This may reflect fusion of small plagioclase inclusions in the original biotite crystals.

We wish to determine the crystallization age of the biotite crystals from the PV-A ash level and have therefore selected the high radiogenic argon (> 60%), high potassium analyses in the middle part of the incremental heating experiment for age calculation (Table 1, Figs. 3, 4). These provided a weighted mean age of 13.32 ± 0.07 Ma (Table 1, Fig. 4), which is concordant with the total fusion and isochron ages. The complete analytical data for the PV-A $^{40}Ar/^{39}Ar$ experiments are available in the supplementary material.

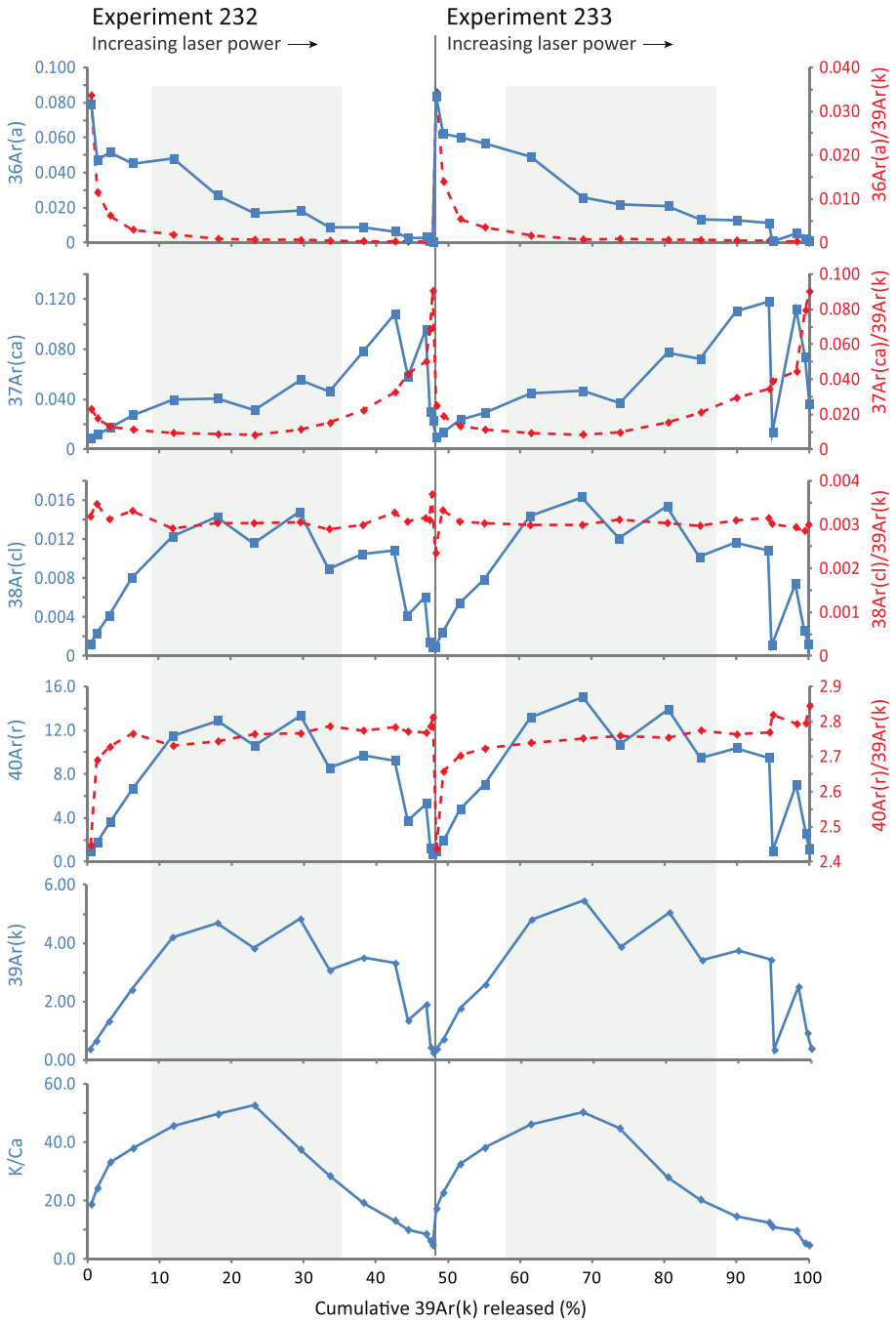

Fig. 3. Degassing diagrams for the $^{40}Ar/^{39}Ar$ experiments. Grey shaded areas indicated the steps included in the weighted mean age. Dashed red lines plotted against axes on the right. Full blue lines plotted against axes on the left. (For interpretation of the references to colour in this figure legend, the reader is referred to the web version of this article.)

4. Paleomagnetic analyses

For magnetostratigraphic purposes, 18 levels were sampled in the 8 m of marine marls above the Badenian evaporites at Piatra Verde using an electrical drill with a generator as power supply. These samples were subjected to either stepwise thermal or alternating field demagnetization, and after each step the Natural Remanent Magnetization (NRM) was measured on a 2G Enterprise horizontal cryogenic magnetometer equipped with DC SQUIDS (noise level 3×10^{-12} Am^2). Thermomagnetic runs were measured in air on a modified horizontal translation type Curie balance with a sensitivity of approximately $\sim 10^{-9}$ Am^2 (Mullender et al., 1993). Measurements were performed up to 700 °C, for selected powdered samples to identify the carriers of the magnetic signal. Approximately 40–60 mg of powdered sample was put into a quartz glass sample holder and held in place by quartz wool; heating and cooling rates were 10 °C/min.

The thermomagnetic runs showed a major increase in magnetization at temperatures of 390–400 °C indicative for the alteration of iron sulphides, such as pyrite, to magnetite (Fig. 5a). Thermal demagnetization was therefore applied to a maximum temperature of 390 °C. Demagnetization diagrams in general show two components: 1) a low-temperature (20–200 °C), low-coercivity (0-20 mT) normal component that we interpret as a viscous component of recent present-day origin and 2) a high-temperature (240–390 °C), high-coercivity (20-60 mT)

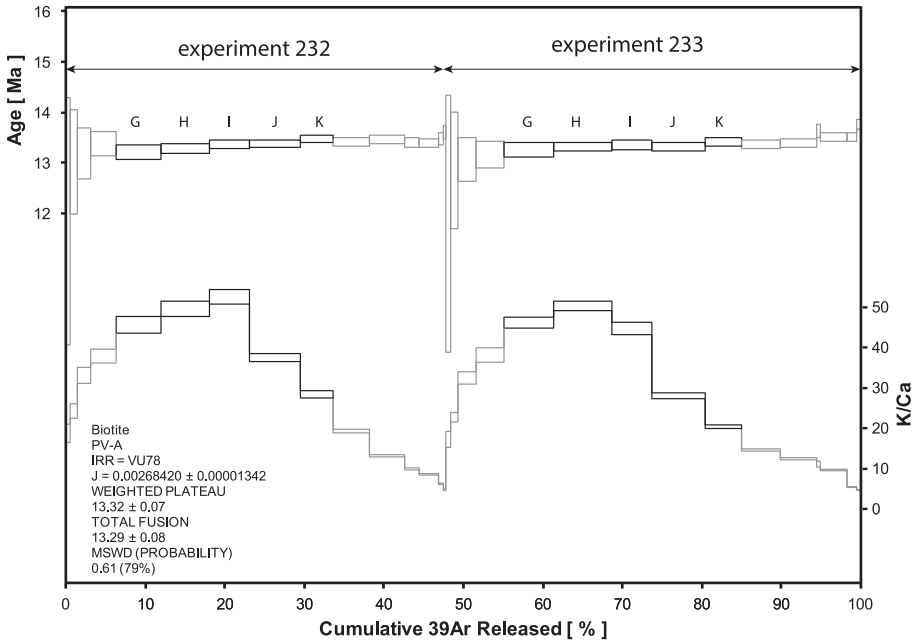

Fig. 4. Weighted mean age and Ca/K ratio for the two $^{40}Ar/^{39}Ar$ experiments. Errors are shown at 1σ.

component of reversed polarity (Fig. 5b). Only the samples from the lowermost stratigraphic level display normal polarity directions (Fig. 5c). We conclude that the magnetic signal in these rocks is most likely carried by greigite, similar to other Paratethys sediments (de Leeuw et al., 2013; Krijgsman et al., 2010; Vasiliev et al., 2010; Vasiliev et al., 2007; Vasiliev et al., 2011). This greigite is interpreted to be of early diagenetic near-primary origin, and we consequently infer that the post-evaporitic marls of Piatra Verde were predominantly deposited during a period of reversed polarity.

5. Integrated biostratigraphy

Twelve micropaleontological samples were collected at regular intervals from the deposits directly overlying the evaporites at Piatra Verde. The samples, which consisted of sandy clay, were disaggregated by boiling in a sodium carbonate solution. They were then washed and sieved over a sieve with a 100 μm mesh. Foraminifera, ostracods, echinoid spines, bryozoans, tube worms, green algae, and fish bones were subsequently hand-picked from the residue under a ZEISS – GSM microscope. In addition, nine sediment samples, taken at regular intervals from the post-evaporitic sediment at Piatra Verde, were analyzed for calcareous nannoplankton, with an Olympus microscope, at ×1200 magnification.

5.1. Foraminifera

Foraminifera are common but generally poorly preserved. The planktonic foraminiferal fauna is composed of the following species: *Globigerinoides trilobus* (Reuss, 1850b), *Paragloborotalia siakensis* (Leroy, 1939), *Globoquadrina altispira* (Cushman and Jarvis, 1936), *Turborotalia apertura* (Cushman, 1918), *Globigerina bulloides* (D'Orbigny, 1826), *Globorotalia transsylvanica* (Popescu, 1970), orbulinids and planoconvex globorotaliids (key species are shown in Fig. 6).

The orbulinids show an incompletely enveloping final chamber with the apertural openings in a polar position. Openings are often stretched rather than circular. Amongst the better preserved specimens are some that show a few openings located away from the intercameral suture and are, therefore, assignable to *Orbulina suturalis* (Brönnimann, 1951). The openings in a few other specimens, however, seem to be confined to the intercameral suture; per definition they thus belong to *Praeorbulina circularis* (Blow, 1956).

The specimens assigned to *P. siakensis* show 4.5–6 chambers in the last whorl, an arched aperture often bordered with a lip, and a small open umbilicus. Sutures on spiral and umbilical side are more or less straight. In all these aspects they compare well with the holotype and topotypes described and figured in Zachariasse and Sudijono (2012).

Interesting are the planoconvex globorotaliids: they resemble both *Globorotalia transsylvanica* (Popescu, 1970) and *Globorotalia partimlabiata* (Ruggieri and Sprovieri, 1970). *Globorotalia transsylvanica* is an endemic species of the Central Paratethys (Popescu and Crihan, 2004), which occurs from the Karpatian up to the late Badenian (Cicha et al., 1998). *Globorotalia partimlabiata* is a marker species for the middle Miocene (Serravallian) in the Mediterranean and North Atlantic (Hilgen et al., 2000). More extensive paleontological studies are required to better understand the taxonomy of these globorotaliids. Here, we conclude that the observed specimens in the Piatra Verde samples correspond to *G. transsylvanica*.

The benthic microfauna is dominated by three species of *Elphidium* (*E. fichtelianum, E.* cf. *eichwaldi* and *E. aculeatum*) with admixtures of *Glabratella platyomphala* and *Lobatula lobatula / Cibicidoides laevi* (key species are shown in Fig. 6). These are mainly epiphytic species (living on algae or sea grass). Deep bottom dwelling species are (almost) absent suggesting that the depositional environment was not very deep. Planktonic foraminifera are abundant, which suggests normal marine conditions in the basin.

5.2. Ostracoda

The most common ostracod taxa recorded in the grey marls above the gypsum at Piatra Verde belong to *Cnestocythere lamellicosta* Triebel, *Loxocorniculum schmidi* (Cernajsek, 1974), *Loxocorniculum hastatum* (Reuss, 1850a), *Loxoconcha punctatella* (Reuss, 1850a), *Loxoconcha kochi* Méhes, *Callistocythere canaliculata* (Reuss, 1850a), *Callistocythere daedalea* (Reuss, 1850a), *Aurila cicatricosa* (Reuss, 1850a), *Phlyctenophora* sp., *Semicytherura* sp., *Heliocythere vejhonensis* (Procházka, 1893), *Tenedocythere sulcatopunctata* (Reuss, 1850a), *Grinioneis haidingeri* (Reuss, 1850a), *Pokornyella deformis* (Reuss, 1850a), *Bairdia subdeltoidea* (Münster, 1830), *Xestoleberis* aff. *Dispar* Muller and *Triebelina boldi* Key (key species are shown in Fig. 6). This ostracod fauna is dominated by shallow water species typical for the Wielician interval of

Table 1
Incremental heating $^{40}Ar/^{39}Ar$ results for biotite from the PV-1 volcanic ash.

Incremental heating			36Ar(a) (V)	37Ar(ca) (V)	38Ar(cl) (V)	39Ar(k) (V)	40Ar(r) (V)	Age ± σ (Ma)	40Ar(r) (%)	39Ar(k) (%)	K/Ca ± 1σ
09M0232C	15.50 W		0.0316786	0.0086449	0.0011997	0.376677	0.92170	11.81 ± 2.45	8.88	0.50	18.7 ± 2.2
09M0232D	18.50 W		0.0189392	0.0116403	0.0022816	0.657650	1.76926	12.98 ± 1.03	23.83	0.87	24.3 ± 1.7
09M0232E	22.00 W		0.0206814	0.0172079	0.0041470	1.328049	3.62220	13.16 ± 0.50	36.97	1.76	33.2 ± 2.0
09M0232F	26.00 W		0.0181177	0.0273120	0.0079836	2.407776	6.65813	13.34 ± 0.24	55.17	3.18	37.9 ± 1.7
09M0232G	30.00 W	×	0.0192022	0.0396680	0.0122715	4.209565	11.49630	13.18 ± 0.16	66.71	5.56	45.6 ± 2.0
09M0232H	34.00 W	×	0.0107588	0.0407251	0.0142620	4.698593	12.89069	13.24 ± 0.10	80.03	6.21	49.6 ± 1.8
09M0232I	38.00 W	×	0.0068066	0.0312674	0.0116057	3.825659	10.57543	13.34 ± 0.09	83.86	5.06	52.6 ± 1.8
09M0232J	44.00 W	×	0.0072789	0.0554025	0.0147880	4.836029	13.37625	13.34 ± 0.08	86.00	6.39	37.5 ± 1.0
09M0232K	50.00 W	×	0.0035028	0.0464391	0.0089091	3.073199	8.56285	13.44 ± 0.08	89.09	4.06	28.5 ± 0.9
09M0232L	60.00 W		0.0034284	0.0779211	0.0104673	3.502593	9.71713	13.38 ± 0.08	90.44	4.63	19.3 ± 0.4
09M0232M	75.00 W		0.0025822	0.1082783	0.0108643	3.320587	9.24362	13.43 ± 0.07	92.28	4.39	13.2 ± 0.3
09M0232N	7.00 W		0.0011059	0.0580143	0.0041506	1.353398	3.75083	13.37 ± 0.09	91.88	1.79	10.0 ± 0.3
09M0232O	9.50 W		0.0011751	0.0956214	0.0060047	1.907916	5.28116	13.35 ± 0.08	93.74	2.52	8.6 ± 0.2
09M0232P	12.00 W		0.0003664	0.0301789	0.0013626	0.439104	1.22353	13.44 ± 0.11	91.77	0.58	6.3 ± 0.2
09M0232Q	15.00 W		0.0002045	0.0231933	0.0009469	0.256447	0.72113	13.57 ± 0.13	92.17	0.34	4.8 ± 0.2
09M0233C	15.50 W		0.0333424	0.0096864	0.0009132	0.388488	0.94659	11.76 ± 2.53	8.68	0.51	17.2 ± 2.0
09M0233D	18.50 W		0.0249730	0.0135654	0.0023801	0.715783	1.90184	12.82 ± 1.14	20.32	0.95	22.7 ± 1.2
09M0233E	22.00 W		0.0240584	0.0234476	0.0054263	1.769914	4.78332	13.04 ± 0.43	39.97	2.34	32.5 ± 1.6
09M0233F	26.00 W		0.0227596	0.0291875	0.0078299	2.585078	7.03833	13.14 ± 0.26	50.87	3.42	38.1 ± 1.8
09M0233G	30.00 W	×	0.0196586	0.0448293	0.0143699	4.811638	13.18088	13.22 ± 0.14	69.18	6.36	46.2 ± 1.4
09M0233H	34.00 W	×	0.0102851	0.0466488	0.0163198	5.456899	15.01859	13.28 ± 0.09	83.00	7.21	50.3 ± 1.2
09M0233I	38.00 W	×	0.0087339	0.0372178	0.0120691	3.876362	10.69749	13.31 ± 0.10	80.38	5.12	44.8 ± 1.5
09M0233J	44.00 W	×	0.0083107	0.0775148	0.0153485	5.055074	13.92277	13.29 ± 0.08	84.85	6.68	28.0 ± 0.7
09M0233K	50.00 W	×	0.0053495	0.0722174	0.0101733	3.421303	9.49319	13.39 ± 0.09	85.58	4.52	20.4 ± 0.5
09M0233L	60.00 W		0.0051664	0.1103572	0.0116332	3.754685	10.37451	13.33 ± 0.08	87.03	4.96	14.6 ± 0.3
09M0233M	75.00 W		0.0044704	0.1182370	0.0108009	3.431896	9.50360	13.36 ± 0.08	87.66	4.54	12.5 ± 0.3
09M0233N	7.00 W		0.0003518	0.0137967	0.0010732	0.355391	1.00185	13.60 ± 0.13	90.49	0.47	11.1 ± 0.7
09M0233O	9.50 W		0.0020630	0.1116736	0.0073941	2.514146	7.02186	13.47 ± 0.08	91.91	3.32	9.7 ± 0.2
09M0233P	12.00 W		0.0007855	0.0735799	0.0026503	0.927401	2.59205	13.48 ± 0.09	91.68	1.23	5.4 ± 0.1
09M0233Q	15.00 W		0.0003058	0.0362012	0.0012048	0.401969	1.14348	13.72 ± 0.10	92.58	0.53	4.8 ± 0.1
		Σ	0.3164427	1.4896750	0.2308312	75.659270	208.43055				

Information on analysis	Results	40(r)/39(k)	± 1σ	Age (Ma)	± 1σ	MSWD	39Ar(k) (%,n)	K/Ca	± 1σ
Sample = VU78–30	Age plateau	2.76130	± 0.00618	13.32	± 0.07	0.61	57.18	30.2 ± 3.6	
Material = Biotite			± 0.22%		± 0.55%	79%	10		
Location = Piatra Verde			Full external error		± 0.16	1.47	1σ confidence limit		
Analyst = Arjan de Leeuw			Analytical error		± 0.03	1.0000	Error magnification		
Project = VU78									
Mass discrimination law = LIN	Total fusion age	2.75486	± 0.00739	13.29	± 0.08		30	21.8 ± 0.1	
Irradiation = VU78			± 0.27%		± 0.57%				
J = 0.00268420 ± 0.00001342			Full external error		± 0.16				
Drachenfels = 25.420 ± 0.163 Ma			Analytical error		± 0.04				

the Badenian (Brestenská and Jiříček, 1978; Gross, 2006). The assemblage suggests a marine, inner shelf environment with a water depth not greater than approximately 100 m.

5.3. Calcareous nannoplankton

The calcareous nannofossil assemblages contained stratigraphically significant species, including *Cyclicargolithus floridanus* (Roth & Hay, *in* Hay et al., 1967) Bukry, 1971 (last common occurrence, LCO at 13.29 Ma), *Calcidiscus premacintyrei* Theodoridis, 1984 (LCO at 12.45 Ma) and *Coronocyclus nitescens* (Kamptner, 1963) Bramlette and Wilcoxon, 1967 (last occurrence, LO at 12.25 Ma), with ages according to Raffi et al. (2006). Other nannofossils that are frequently present in the samples are *Discoaster exilis* Martini and Bramlette, 1963, *D. variabilis* Martini and Bramlette, 1963, *Sphenolithus moriformis* (Brönnimann and Stradner, 1960), Bramlette and Wilcoxon, 1967, *Calcidiscus leptoporus* (Murray and Blackman, 1898), Loeblich Jr. and Tappan, 1978, *C. macintyrei* (Bukry and Bramlette, 1969) Loeblich Jr. and Tappan, 1978, *Helicosphaera carteri* (Wallich, 1877) Kamptner, 1954, *Coccolithus pelagicus* (Wallich, 1877), Schiller, 1930 and *Braarudosphaera bigelowii* (Gran and Braarud, 1935) Deflandre, 1947 (Fig. 6).

All the studied samples belong to the NN6 calcareous nannoplankton zone of Martini (1971), which covers the time interval between the LO (last occurrence) of *Sphenolithus heteromorphus* Deflandre, 1953 and the FO (first occurrence) of *Discoaster kugleri* Martini and Bramlette, 1963. *Sphenolithus heteromorphus* is not present in any of the investigated samples and they are thus inferred to have been deposited after the LO of the aforementioned nannofossil, which is dated at 13.54 Ma in the West Atlantic and 13.64 Ma in the Eastern Mediterranean (Raffi et al., 2006). The presence of abundant calcareous nannofossils suggests that surface waters and probably the upper part of the water column were subject to normal open-marine conditions.

6. Discussion

6.1. Age of the termination of the BSC in the Slănic Syncline

Our results provide new chronologic constraints on the termination of the BSC. The $^{40}Ar/^{39}Ar$ results provide a 13.32 ± 0.07 Ma weighted mean age (Fig. 4) for the PV-A tuff level that is intercalated with marls that concordantly overlie clastic BSC gypsum deposits in the investigated outcrop (Fig. 1). Magnetostratigraphic analyses (Fig. 5) show that the marl succession, in which the tuff is intercalated, was predominantly deposited during a period of reversed polarity. Based on the

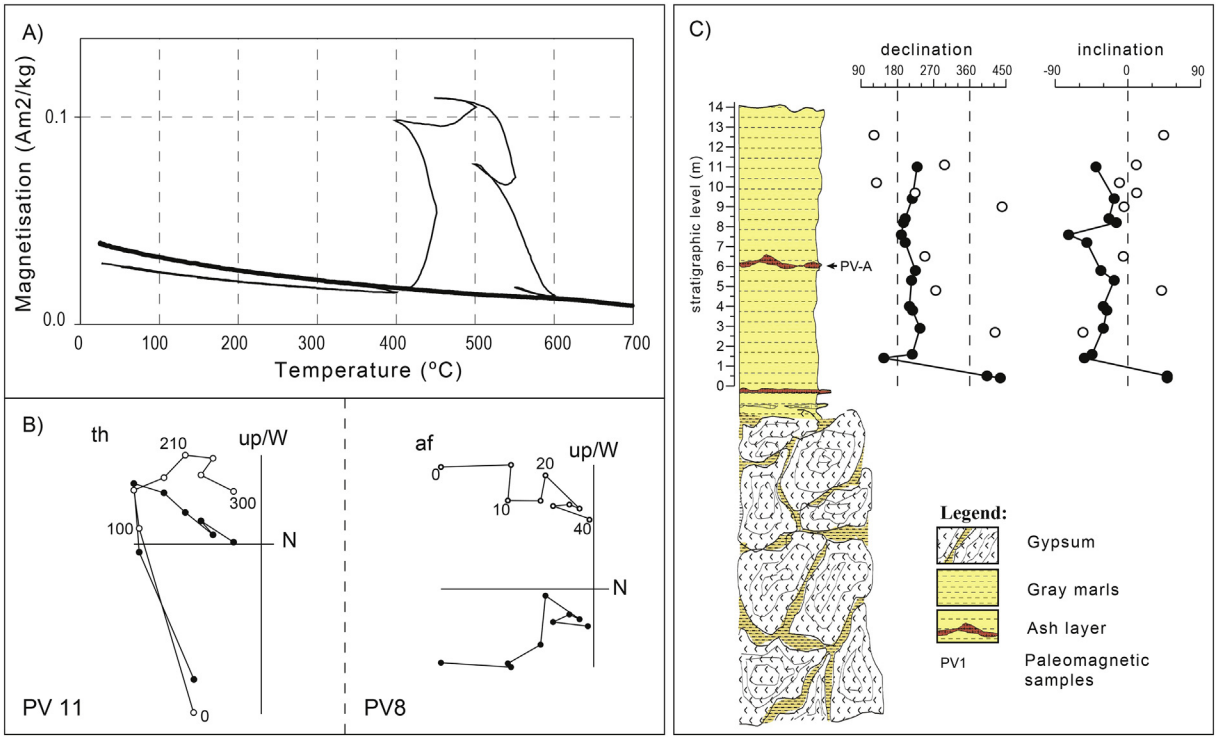

Fig. 5. Paleomagnetic results: a) Thermomagnetic runs in air. b) Demagnetization diagrams. c) Magnetostratigraphy for the investigated section. PV-A is the dated ash layer.

above mentioned 13.32 ± 0.07 Ma $^{40}Ar/^{39}Ar$ age, this reversed period corresponds to chron C5AAr of the GPTS, which according to Hilgen et al. (2012) lasted from 13.363 Ma to 13.183 Ma (Fig. 7). Ostracods, planktonic and benthic foraminifera indicate that the investigated marls accumulated in a shallow, normal marine basinal environment relatively distal to clastic sediment input. We thus infer from these results that by 13.32 ± 0.07 Ma gypsum reworking had ended and deposition of marls with abundant microfauna had resumed at Piatra Verde. We interpret this switch to normal marine conditions to signify the end of the BSC in the area of the Slănic syncline.

6.2. Biostratigraphic position of the marls overlying the BSC gypsum

The paleontological assemblages from the studied outcrop at Piatra Verde allow regional (Paratethys) and global biostratigraphic correlation. The nannofossil data show that the marl unit at Piatra Verde belongs to the NN6 calcareous nannoplankton zone of Martini (1971) which covers the time interval between 13.53 and 11.86 Ma (Gradstein et al., 2012). This is in agreement with the obtained radio-isotopic age and with other nannoplankton studies from the Carpathian Foredeep (Andreyeva-Grigorovich et al., 2003; Mărunţeanu, 1999; Peryt, 1997; Peryt, 1999) and the Transylvanian Basin (Chira, 2000). Globally, the NN6 zone covers part of the Serravallian (Raffi et al., 2006; Gradstein et al., 2012). The same nannofossil assemblages as identified here from Piatra Verde in the Romanian Carpathians were reported from the GSSP of the Serravallian (Hilgen et al., 2009), where the LO of *Sphenolithus heteromorphus* is followed by the LCO of *Cyclicargolithus floridanus*.

The overall composition of the planktonic foraminiferal fauna is also very similar to that of time-equivalent Serravallian sections in the Mediterranean (pers. com. J.W. Zachariasse). The joint presence of *O. suturalis* and *P. siakensis* suggests deposition between 15.10 and 11.19 Ma (being the ages for the First Occurrence (FO) of *O. suturalis* (Berggren et al., 1995) and the Last Occurrence (LO) of *P. siakensis* in the Mediterranean (Hilgen et al., 2003). The poor preservation of the planktonic index species makes it difficult to correlate the investigated deposits in more detail to the Serravallian biostratigraphic scale of the Mediterranean (Hilgen et al., 2009).

The obtained radio-isotopic age constraint helps to resolve the ambiguity in the planoconvex globorotaliids in our samples that resemble both *Globorotalia transsylvanica* (Popescu, 1970) and *Globorotalia partimlabiata* (Ruggieri and Sprovieri, 1970). *Globorotalia partimlabiata* is a marker species for the middle Miocene (Serravallian and Tortonian) in the Mediterranean and North Atlantic (Hilgen et al., 2000). It there occurs from 12.88 Ma (Abels et al., 2005) to 9.94 Ma (Hilgen et al., 2000). Given the 13.32 Ma age constraint for the Piatra Verde tuff layer, we conclude that the globorotaliids in our section (Fig. 6) must in fact be *G. transsylvanica.* This species is endemic to the Central Paratethys and occurs from the Karpatian to the late Badenian, but it is most abundant in the Moravian and Wielician intervals of the Badenian (Popescu, 1987; Cicha et al., 1998; Popescu and Crihan, 2011; Filipescu and Filipescu, 2015).

The presence of the planktonic foraminifer species *Globoturborotalita druryi* (Akers, 1955) and the benthic foraminifera species *Uvigerina orbignyana* Czjzek, in combination with the absence of foraminifera particular for the Late Badenian (Kosovian) *Velapertina indigena* zone, indicate that the investigated deposits overlying the evaporites belong to the middle part of the regional Badenian stage, which is in this area traditionally known as the Wielician (Popescu, 1987; Krézsek and Filipescu, 2005; Popescu and Crihan, 2011; Gonera, 2013). Our results highlight that a Wielician-type microfossil assemblage is still present in the stratigraphic interval directly overlying the BSC evaporites at Piatra Verde. This is in line with the Badenian stratigraphic scheme compiled by Gonera (2013).

In conclusion, the marls overlying the gypsum at Piatra Verde belong to the Wielician interval of the regional Badenian stage, the NN6 calcareous nannoplankton zone and the Serravallian stage of the Standard Geological Timescale.

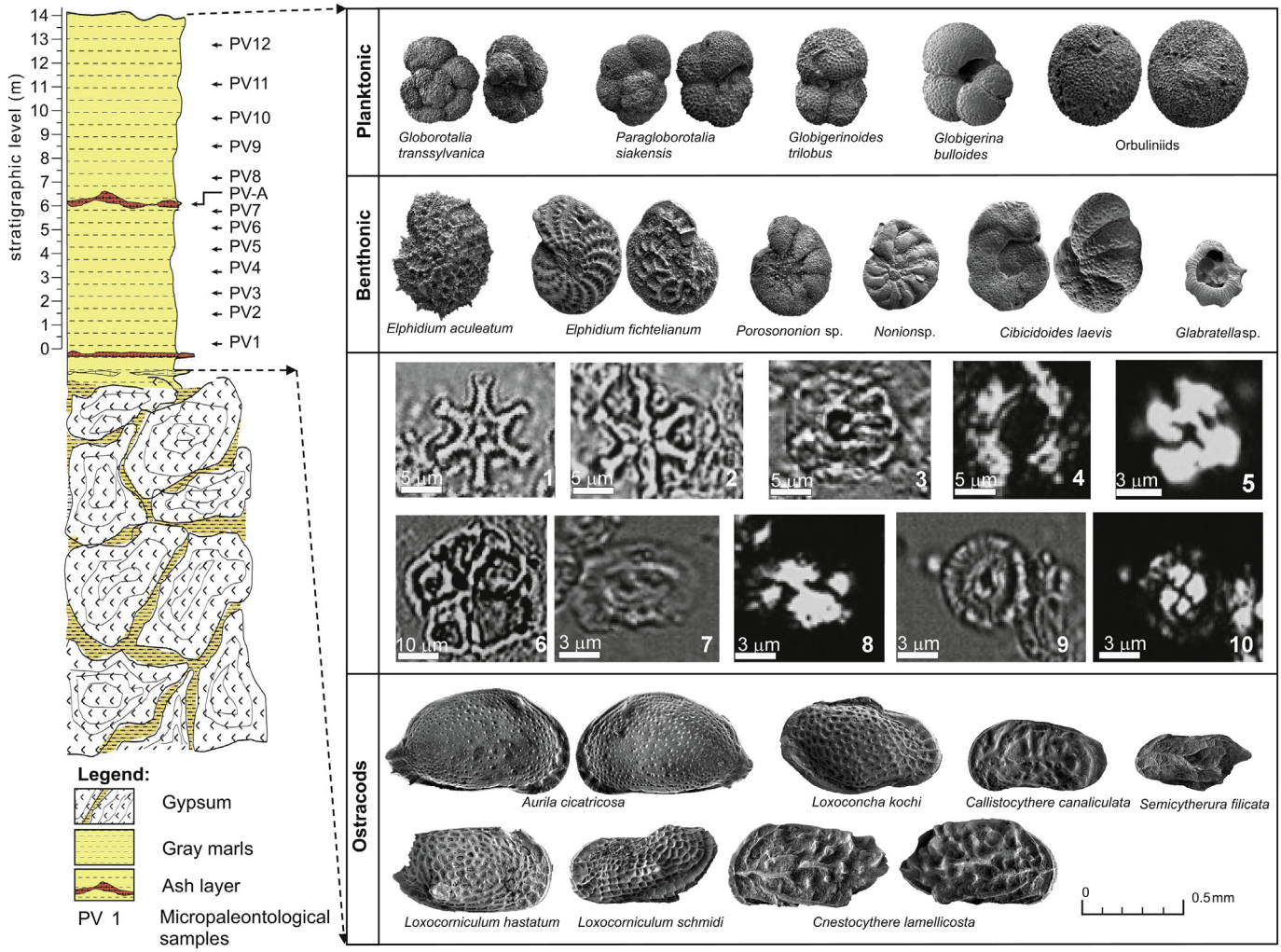

Fig. 6. Plates with key foraminifera, ostracodes and nannofossils from the studied section. Ostracod and foraminifera taxa are indicated on the figure. Nannofossils are: **1–2**: *Discoaster variabilis* Martini and Bramlette, 1963; **3**, **4**: *Calcidiscus macintyrei* (Bukry and Bramlette, 1969) Loeblich Jr. and Tappan, 1978; **5**: *Cyclicargolithus floridanus* (Hay et al., 1967) Bukry, 1971; **6**: *Braarudosphaera bigelowii* Deflandre, 1947; **7–8**: *Helicosphaera carteri* (Wallich, 1877) Kamptner, 1954; **9–10**: *Calcidiscus leptoporus centrovalis* (Stradner & Fuchs, 1980) Perch-Nielsen, 1984. All nannofossil microphotographs were taken with a LM (light microscope); 1–3, 6–7 and 9 - transmitted light; Figs. 4-5, 8 and 10 - crossed nicols.

6.3. Comparison with radio-isotopic age constraints on BSC termination in Poland and Ukraine

Several $^{40}Ar/^{39}Ar$ ages have recently been determined for post-BSC deposits in Poland and Ukraine, which are complementary to our results from Piatra Verde and need to be compared. The Badenian stratigraphy of the Carpathian Foredeep in Ukraine and Poland strongly resembles the Badenian Stratigraphy of the Romanian East Carpathians, although the local terminology differs (Fig. 7).

Śliwiński et al. (2012) have provided $^{40}Ar/^{39}Ar$ ages for the Babczyn Tuff, which is intercalated in the Pecten Beds. These consist of clays and marls with abundant pectinids that unconformably overlie the BSC gypsum along the northern, marginal part of the Polish Carpathian foreland basin. They range in thickness from several to over 40 m and contain late Badenian (Kosovian) index fossils including *Flexopecten lilli* (Push), *Palliolum bittneri* (Toula) and *Limacina gramensis* (Rasmussen) and are thus biostratigraphically younger than the here investigated Wielician marls at Piatra Verde (Fig. 7).

The Pecten Beds bear intercalations of clastic gypsum which indicates that the marginal gypsum was partially eroded before and during deposition (Śliwiński et al., 2012). The abundance of *Pecten* decreases basinwards (i.e. to the south and southeast), where the Pecten Beds laterally grade into the Spirialis Clays (30–80 m thick, with abundant pteropods). These could be considered equivalent to the Spirialis Marls of the Romanian East Carpathians (Fig. 7). To the northeast of Kraków, deposits containing pteropods and *Radiolaria* – designated as the 'Radiolaria horizon' – are intercalated between the Pecten Beds and the gypsum deposits (Barwicz-Piskorz, 1978; Barwicz-Piskorz, 1997; Osmólski, 1972). This 'horizon' belongs to the late Badenian *Velapertina indigena* foraminiferal Zone and may be equivalent to the Radiolarian Shales in Romania. The faunal assemblage of the Pecten Beds indicates deposition in a normal marine (neritic, several tens of meters deep) setting in basinal environments with wide prodeltas receiving sediment from suspension plumes and by storm surge-related and density-turbidity currents (Śliwiński et al., 2012). The coeval Spirialis Clays were also interpreted as prodeltaic facies.

$^{40}Ar/^{39}Ar$ dating of biotite and volcanic glass from the rhyolitic Babczyn Tuff provided an age of 13.06 ± 0.11 Ma (Śliwiński et al., 2012). However, the $^{40}Ar/^{39}Ar$ method is inherently a relative technique: It determines the age of an unknown sample relative to the age of a known standard. There is a large set of different standards in use and these have widely varying ages. Ages attributed to a single standard also differ across publications. In order to properly compare $^{40}Ar/^{39}Ar$ ages, they need to be recalibrated to the same standard ages (Renne et al., 1998). The ages reported in the current paper and in de Leeuw et al. (2010) and Bukowski et al. (2010) were determined relative to the

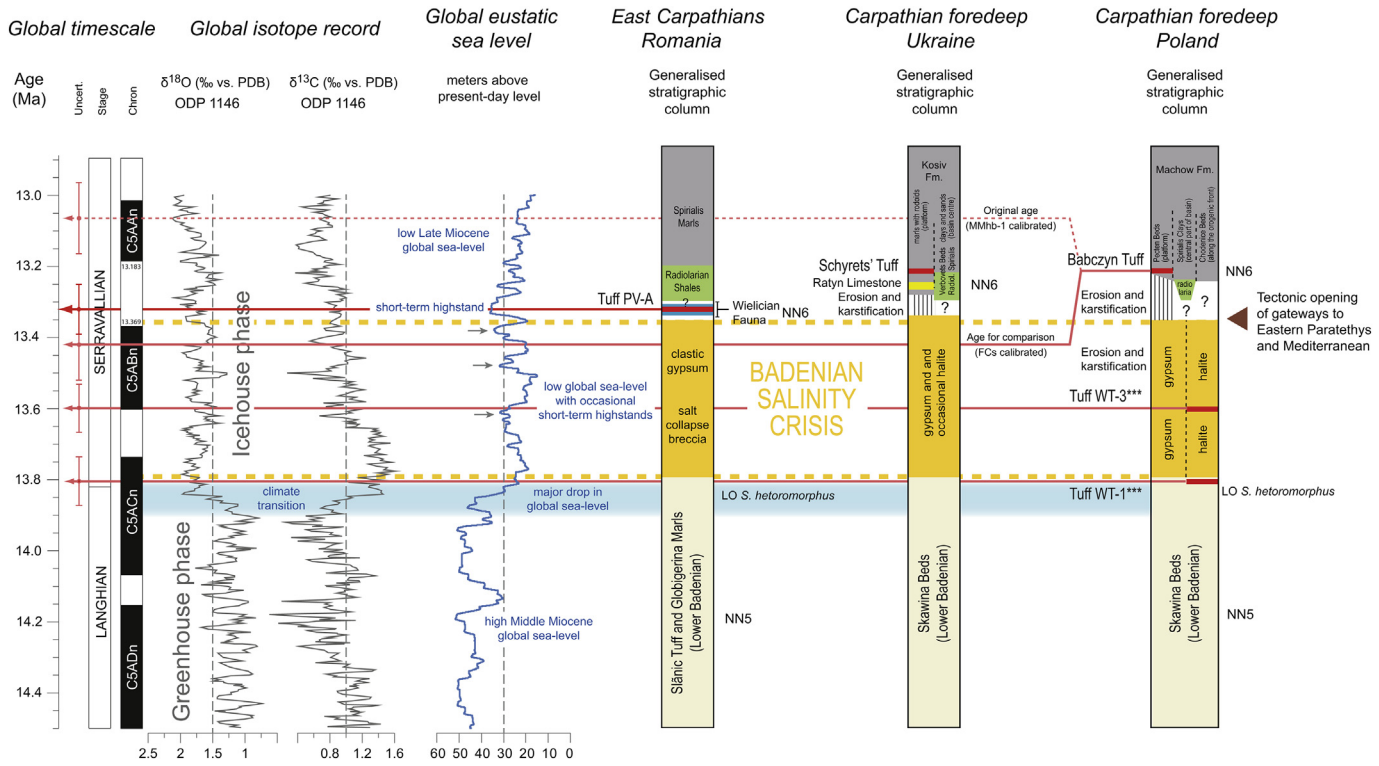

Fig. 7. Tentative correlation of BSC related deposits based on our new results and Śliwiński et al. (2012), Andreyeva-Grigorovich et al. (2003), Peryt et al. (2014) and Peryt and Peryt (2009). Global timescale according to Gradstein et al. (2012). Stable oxygen and carbon isotope data are from Ocean Drilling Program (ODP) Site 1146 in Caribbean (Holbourn et al., 2007). Global eustatic sea level is according to modelling studies by de Boer et al., 2010who derive global eustatic sea level from ice volume. We refrain from using the $^{40}Ar/^{39}Ar$ age of the Schyrets tuff (Nejbert et al., 2012), because insufficient data are available for recalibration to FCs.

28.201 ± 0.046 Ma astronomically tuned age for Fish Canyon Tuff sanidine (FCs; Kuiper et al., 2008), using the decay constant of Steiger and Jäger (1977). Both the FCs and the volcanic ashes below and above the BSC are Miocene in age. Standards with ages comparable to those of the unknowns are necessary in order to reduce the dynamic range of isotopic ratios to be measured (Renne et al., 1998). Using the astronomically tuned age for FCs furthermore increases the compatibility of the obtained ages with the global standard timescale for the Miocene, which is also astronomically tuned (Hilgen et al., 2012). The 13.06 ± 0.11 Ma age for the Babczyn Tuff was determined relative to a Cambrian 513.9 ± 2.30 Ma age for the MMhb-1 hornblende standard (Lanphere et al., 1990; Śliwiński et al., 2012). The reported age can be recalibrated to the astronomically tuned age of FCs using:

$$t_{Babczyn\_recal} = \frac{1}{\lambda} ln((e^{\lambda t_{FCs}} - 1) R_{FCs}^{MMhb-1} R_{MMhb-1}^{Babczyn} + 1)$$

where $t_{Babczyn\_recal}$ is the recalibrated age of the Babczyn Tuff, λ is the decay constant according to Steiger and Jäger (1977), t_{FCs} is the 28.201 ± 0.046 Ma astronomically tuned age of the FCs standard and R_{FCs}^{MMhb-1} is the intercalibration factor between the FCs and MMhb-1 standards determined by Renne et al. (1998). $R_{MMhb-1}^{Babczyn}$ can be calculated from the results reported by Śliwiński et al. (2012) using:

$$R_{MMhb-1}^{Babczyn} = \frac{(e^{\lambda_s t_{Babczyn\_orig}} - 1)}{(e^{\lambda_s t_{MMhb-1}} - 1)}$$

Where λ is the decay constant used in Śliwiński et al. (2012), which is in this case also according to Steiger and Jäger (1977), $t_{Babczyn\_orig}$ is the 13.06 ± 0.11 Ma age of the Babczyn tuff reported by Śliwiński et al. (2012) and t_{MMhb-1} is the 513.9 ± 2.30 Ma age that was attributed to the MMhb-1 standard. Error calculation follows Renne et al. (1998). Accordingly, the recalibrated Babczyn Tuff age is 13.41 ± 0.10 Ma. Since this age for the Babczyn Tuff is now calibrated against the same astronomically tuned FCs standard that is used in the current paper, it may be compared with our results directly.

Another age constraint for the end of the BSC is provided by recent $^{40}Ar/^{39}Ar$ ages for glass shards from the Chodenice Tuff from the radiolaria-bearing Chodenice Beds overlying the salt of the Wielicka Beds near Bochnia in Poland (Bukowski et al., 2010). However, the obtained 13.62 ± 0.10 age for these post-BSC deposits is in conflict with the 13.60 ± 0.07 Ma age obtained by the same research group for a tuff present within the evaporitic deposits (de Leeuw et al., 2010). Both papers use the same standards and decay constants as used in the current paper, which facilitates comparison. The Chodenice result was in this case considered less reliable, because it was obtained on glass shards and hydration resulting in mobility of K and/or Ar in glass, and recoil artefacts produced by neutron irradiation, can severely affect glass shards from volcanic ashes (Morgan et al., 2009). The Chodenice Tuff therefore does not provide a reliable age for the end of the BSC.

Finally, a $^{40}Ar/^{39}Ar$ age was recently obtained for volcanic glass from a thin (2 cm) pyroclastic deposit within late Badenian marine marls of the Kosiv Fm. that overlies BSC gypsum at Schyrets in the Ukrainian Carpathian foreland basin (Fig. 7; Nejbert et al., 2012). Regionally, the Kosiv Fm. consists of silty grey clays with interbeds of silt, sandstone, tuff, and tuffites (Andreyeva-Grigorovich et al., 1997). The lower part of the formation is known as the Verbovets Beds that contain numerous *Globigerina bulloides* d'Orbigny, *G. regularis* d'Orbigny, *Subbotina cognata* (Pishvanova), and *Velapertina indigena* (Luczkowska). Radiolarians occur in the lower part of the Verbovets Beds, while pteropods of the genus *Spiratella*, and foraminifera occur in their upper part (Garecka and Olszewska, 2011). This invokes an analogy with the Radiolarian Shales and Spirialis Marls of the Romanian East Carpathians (Fig. 7). Detailed investigations revealed a high degree of similarity of foraminiferal assemblages of the *Pecten/Spirialis* beds of Poland and the Kosiv Fm. of Ukraine (Garecka and Olszewska, 2011). Assemblages from both areas are characterized by numerous arenaceous species of foraminifera and, in particular, late Badenian

(Kosovian) index planktonic species *Velapertina indigena* (Garecka and Olszewska, 2011). Both foraminiferal and dinoflagellate cyst assemblages indicate an open marine shelf to bathyal environment with normal-marine salinity and cool waters (Peryt et al., 2014). Again, it is apparent that there is a high degree of similarity in the Badenian stratigraphy of the Ukrainian Carpathian Foredeep and the outer part of the Romanian East Carpathians. Unfortunately, insufficient data were reported in Nejbert et al. (2012) for recalibration of the 13.19 ± 0.14 Ma age for the Schyrets Tuff to the FCs standard. We therefore refrain from a direct comparison with our results.

In summary, the end of the BSC is currently constrained by two $^{40}Ar/^{39}Ar$ ages: the 13.41 ± 0.10 Ma age of the Babczyn Tuff in Poland and our 13.32 ± 0.07 Ma age for the PV-A tuff from Piatra Verde in Romania. The listed ages are both calibrated against the astronomically tuned age of FCs and are statistically overlapping. The marls in which the PV-A tuff occurs have a reversed polarity, whereas magnetostratigraphic results for the post-BSC deposits in the North Carpathian Foredeep of Poland are inconclusive because of the presence of a pervasive late diagenetic (normal polarity) overprint of the magnetic signal (Sant et al., 2015). In the light of these data, we consider it most likely that the BSC ended in the lower part of chron C5AAr around 13.35 Ma in the Romanian East Carpathians as well as in the Polish Carpathian Foredeep.

There is a discrepancy in the relative ages of the Babczyn and PV-A ashes in comparison with biostratigraphic data (Fig. 7.). This is probably attributable to the use of the Cambrian age MMhb-1 standard to date the Miocene Babczyn tuff, which has likely introduced additional uncertainty not properly reflected in the expressed ± 0.010 Ma confidence interval. It is furthermore known that the MMhb-1 standard is inhomogeneous (Renne et al., 1998), which results in additional uncertainties. This shows that caution is required when determining $^{40}Ar/^{39}Ar$ ages, because these ages are not absolute, but inherently linked to the age of the standard used for comparison (Renne et al., 1998). It would be interesting to date the Babczyn, Schyrets and PV-A ashes in a single experiment, so external sources of error can be excluded when their ages are compared.

6.4. What terminated the BSC?

The open marine faunal assemblages of the marls that overlie the Badenian gypsum deposits at Piatra Verde indicate that the BSC was terminated by a regional transgression, i.e. a relative rise in sea-level. In combination with sedimentological and paleontological data from the Polish and Ukrainian parts of the Carpathian Foredeep, the following scenario is suggested: In the final stages of the BSC, gypsum beds that previously accumulated along the basin margins became exposed, leading to reworking of clastic gypsum into the deeper basin. Gypsum reworking was ended by a marine transgression in the area of the Slănic Syncline just prior to 13.32 ± 0.07 Ma. Our results indicate that the oldest transgressive deposits still have a typical Wielician-type microfauna alongside an NN6 nannofossil assemblage. Base-level increased further in the Late Badenian (early Kosovian interval, *Velapertina indigena* zone) and distal deposits with abundant radiolarians accumulated, possibly due to mass mortality events triggered by turnovers in the water column (Peryt, 2006). These radiolarian bearing deposits are not only present in the Romanian East Carpathians, but also in the Ukrainian and Polish foreland (Barwicz-Piskorz, 1978; Barwicz-Piskorz, 1997; Osmólski, 1972). This suggests that, by the early Kosovian, relative base-level had risen to such an extent that a deeper water marine environment was present in the Ukrainian and Polish Carpathian foreland. It is not clear if the contact between the evaporites and the overlying Kosiv and Machow fms. is unconformable in this area and it is therefore difficult to say if the basin center became exposed during the final stages of the BSC. Following deposition of the radiolarian beds, distal deposits with abundant pteropods (*Spirialis/Spiratella*) accumulated in the central part of the basin. These graded into more proximal deposits with *Pecten* towards the basin margin along the European Platform. In the Polish foreland, these Pecten beds gradually onlapped the formerly exposed gypsum deposits.

The main question currently to be resolve is if the transgression that ended the BSC was related to a global rise in eustatic sea-level, or if it was caused by regional tectonic events. The frequently used sequence stratigraphic compilations of Miller et al. (2005), Browning et al. (2008) and Kamp et al. (2004) are too fragmentary and/or low in detail to resolve global sea-level variations at the required resolution. The global eustatic sea-level reconstruction based on ice-volume modelling of de Boer et al., 2010is both detailed and continuous enough to be informative. It shows generally high global eustatic sea-level during the Langhian, with a sharp transition to the generally low Serravallian sea levels just prior to 13.8 Ma (Fig. 7). This corroborates the inference that the onset of the BSC at 13.81 Ma might have been triggered by global-cooling-induced base-level lowering that restricted the Central Paratethys (de Leeuw et al., 2010) and the Eastern Paratethys (Palcu et al., 2017). Global sea-level generally remained low during the BSC (Fig. 7). Some of the modeled short-term global highstands (Fig. 7) may have temporarily increased the connectivity of the Central Paratethys with the global ocean during the BSC, leading to a decrease in its salinity. This could explain some short-lived return of normal marine foraminifera (e.g. Borków section in Poland, (Peryt, 2013a). The model output of de Boer et al. (2010) does reveal a slightly more prominent global sea-level highstand that is reached at 13.33 Ma. In itself, this short-term (30 kyr) highstand would only have led to another short-lived, temporary connection between the Central Paratethys and the Mediterranean. However, at 13.25 Ma global eustatic sea-level returned to, and remained at values that were as low as during the BSC, yet evaporite deposition in the Central Paratethys did not resume. This indicates that changes in global sea-level had only a minor influence on the termination of the BSC.

Improved interconnectivity with the neighbouring Eastern Paratethys and/or Mediterranean due to tectonic lowering of the intervening gateway(s) best explains why evaporite precipitation did not resume despite the generally low global sea-level in the 300 kyr following the BSC. It is in this respect interesting to note that the onlap of post-BSC deposits onto the European Platform does not necessarily reflect a eustatic global base-level rise, but more likely relates to expansion of the foreland basin towards the passive margin due to progressive orogenic loading and lithospheric flexure. This is also the likely reason why BSC gypsum, thought to have accumulated during a base-level lowstand, in places directly overlies the Mesozoic or Palaeozoic of the platform (Peryt et al., 2012). This idea is corroborated by an influx of 20% Central Paratethyan species into the Eastern Paratethys during the Konkian (Serravallian) transgression (Kováč et al., 2007 and references therein), which ended the Karaganian isolation of the Eastern Paratethys at 13.4 Ma (Palcu et al., 2017). In any case, the Outer Carpathian accretionary wedge was actively forming during the Badenian all along the Western and Eastern Carpathians (Kováč et al., 2007). Regional profiles in front of the Romanian East Carpathians demonstrate the onset of flexural subsidence during the Late Badenian (Matenco et al., 2003). Expansion of the Carpathian foreland basin towards the platform may thus have generated or widened a connection with the Eastern Paratethys through present-day southern Ukraine and the Republic of Moldavia, just to the north of the current Danube Delta. This is in agreement with conclusions drawn by Palcu et al. (2017) based on Badenian fossil assemblages of Eastern Paratethys and sediments in the gateway area. Thin intervals (< 2 m) of Late Badenian sediments also occur locally in South Dobrogea, which may hint at an additional gateway in this area.

The similarity of the overall composition of the planktonic foraminiferal fauna in the investigated section to that of time-equivalent sections in the Mediterranean nevertheless strongly suggests that, in addition to the connection to the Eastern Paratethys, there was a connection between the Mediterranean and the Central Paratethys

following the BSC. This is in line with a comparative calcareous nannoplankton study of Bartol et al. (2014), which reveals both Mediterranean and Eastern Paratethyan influences throughout the entire Central Paratethys during the late Badenian. This is also in agreement with a strong species level affinity between conoideans from late Badenian reefs in the Ukrainian Carpathian foreland basin and the Mediterranean-Atlantic (Scarponi et al., 2016). The gateway between the Mediterranean and the Central Paratethys is thought to have been located in present-day Slovenia (Fig. 1) (Bartol et al., 2014), although some alternative hypotheses exist (references in Kováč et al., 2007). Progressive rifting in the Pannonian Basin System during the Badenian may have improved water circulation from the western part of the Central Paratethys to the Carpathian Foreland, thereby preventing renewed evaporite formation.

6.5. Uncertainties and outstanding questions

Our results show that evaporite deposition had ended by 13.32 ± 0.07 Ma in the Slănic Syncline, but several outstanding questions remain, especially regarding the evolution of the BSC in the Slănic Syncline and the wider South and East Carpathian foreland basin area. In general, there is a need for a more detailed description and palaeo-environmental interpretation of the BSC succession in the East Carpathians.

More in particular, a better insight in the genesis of the Cosmina Breccia is essential for our understanding of the BSC in the study area. The structure of the Cosmina Breccia, as evident from the geological map (Fig. 2), suggests that it concerns a salt collapse breccia (cf. Peryt, 2006). A salt-collapse breccia implies that salt would originally have been present between the two gypsum intervals: There is selenitic gypsum present below the Cosmina Breccia in Valea Rea (Frunzescu, 2005 and authors own observations) and above at Piatra Verde. An alternative interpretation is that it formed as a sedimentary breccia with large olistoliths (Frunzescu, 2005; Frunzescu, 2010). In that case salt precipitation may not have taken place in this area.

Another unresolved question concerns the exact age of the salt deposits in the South and the East Carpathians. The established view is that there are several evaporite horizons; two in the early Miocene, (Motaş et al., 1966), one in the Badenian (Popescu, 1951; Motaş et al., 1966; Frunzescu, 2012) and one in the Sarmatian (Frunzescu et al., 2010). Outcrop evidence shows that gypsum strata are indeed present in all intervals. Salt is diapiric in the Carpathians and frequently dissolved into salt breccias at the surface which makes it more difficult to constrain its age. The salt in the Slănic Syncline and adjacent Prahova Valley is interpreted to be Badenian in age on the geological map (Murgeanu et al., 1967). This also holds for the diapirs along the Băicoi-Moreni alignment, but these have recently been re-interpreted to be of early Miocene age based on seismic data (Schleder et al., 2016). The presumed Badenian salt in the Câmpina area is positioned adjacent to a thrust and occurs below the Slănic Tuff near Doftana (Murgeanu et al., 1967), which might be consistent with a diapiric origin from an early Miocene stratigraphic level. It raises the question whether the Slănic Prahova salt is stratigraphically in place, or that it may have risen up from the early Miocene along strike slip faults that have affected the basin (Murgeanu et al., 1967; Ștefănescu et al., 1978).

A final issue that needs to be addressed in the future is the age of the last occurrence (LO) of the calcareous nannofossil *Sphenolitus heteromorphus* in the Central Paratethys. The last occurrence of *S. heteromorphus* is demonstrably diachronous around the world and was dated at 13.532 Ma in the Central Atlantic and at 13.654 Ma in the Mediterranean (Raffi et al., 2006). Recent research has shown that the last occurrence of this guide fossil that defines the NN5/NN6 zone boundary, is located below the BSC evaporites in Poland (Peryt, 1997) as well as at Piatra Verde in Romania (Melinte-Dobrinescu and Stoica, 2014). $^{40}Ar/^{39}Ar$ dating of a volcanic ash just below the evaporites in Poland indicates that BSC evaporite deposition started just after 13.81 ± 0.08 Ma (Fig. 7; de Leeuw et al., 2010). Since *S. heteromorphus* disappears from the calcareous nannofossil assemblages below the BSC evaporites, its last occurrence might be 160 kyr older in the Central Paratethys than in the Mediterranean. This would also imply that the LO of *S. heteromorphus* might be located below the Mi3b isotope excursion in this region. However, at the resolution of 160 kyr uncertainties in the radio-isotopic ages evidently play a role. Consequently, this issue needs to be tackled with integrated biostratigraphic, magnetostratigraphic, radio-isotopic, and stable isotope research.

7. Conclusions

In a classical succession at Piatra Verde in the Slănic Syncline in the East Carpathians, reworked BSC gypsum deposits are overlain by 15 m of marls with some intercalating volcanic tuffs (Fig. 1, Fig. 2). A weighted mean $^{40}Ar/^{39}Ar$ age of 13.32 ± 0.07 Ma was obtained for biotite separates obtained from one of these tuffs, located ~6 m above the top of the BSC evaporites (Fig. 4). Paleomagnetic analyses indicate that the marls were deposited during a period of reversed polarity (Fig. 5), which correlates with C5AAr of the GPTS. This is in line with our calcareous nannoplankton results that are indicative of NN6 (Fig. 6), which spans part of the Serravallian. Both foraminifera and ostracods are typical for the Wielician interval of the regional Badenian stage. Ostracods and foraminifera further indicate that the investigated marls accumulated in a shallow, normal marine basinal environment relatively distal to clastic sediment input. We thus infer that by 13.32 ± 0.07 Ma the BSC had ended in the area of the Slănic Syncline. The obtained age statistically overlaps with complementary recalibrated $^{40}Ar/^{39}Ar$ results of Śliwiński et al. (2012) from the post-BSC Pecten Beds in Poland. In combination with previously obtained radio-isotopic constraints on the onset of the BSC in Poland (de Leeuw et al., 2010), our results constrain the duration of the BSC to a maximum of 500 kyr (Fig. 7).

This age framework helps to clarify allogenic controls on the termination of the BSC. High-resolution ice-volume modelling of de Boer et al. (2010) shows a relatively low middle Badenian global eustatic sea-level with some short-term peaks that may have led to temporary return of normal marine conditions in the Badenian evaporite basin during the BSC. Following the last of these short-term highstands (13.33–13.25 Ma), g global eustatic sea-level returned to, and remained at values that were as low as during the BSC, yet evaporite deposition in the Central Paratethys did not resume. On the contrary, a basin-wide transgression and the exchange of water and fauna between the Central Paratethys, the Eastern Paratethys and the Mediterranean followed. We deduce that the intervening barriers between these basins must have been lowered by tectonic processes. Flexural subsidence of the East Carpathian Foreland in the area of present day Moldova and South Ukraine likely enhanced the gateway to the Black Sea Basin, while progressive rifting in the Pannonian Basin may have improved the exchange of water with the Mediterranean. In conclusion, we infer from our obtained age framework and paleontological results that the termination of the BSC cannot be attributed to global eustacy, but was due to tectonic lowering of the barriers between the Central Paratethys and the neighbouring basins.

Supplementary data to this article can be found online at https://doi.org/10.1016/j.gloplacha.2018.07.001.

Acknowledgements

We thank Roel van Elsas for assistance with mineral separation. Jan Wijbrans and Michael Flowerdew are thanked for discussion of the $^{40}Ar/^{39}Ar$ results. Erik Snel has performed the paleomagnetic analyses. Monica Crihan, Gheorghe Popescu and Jan-Willem Zachariasse helped with the identification of the foraminifera. We are grateful to Michel Kováč, Jean-Pierre Suc, the editor and three anonymous reviewers for their suggestions and comments which have helped to improve this

article. This research was supported by the Netherlands Research Centre for Integrated Solid Earth Sciences (ISES) and by the Netherlands Geosciences Foundation (ALW) with support from the Netherlands Organization for Scientific Research (NWO) through the VICI grant of WK.

References

Abels, H.A., Hilgen, F.J., Krijgsman, W., Kruk, R.W., Raffi, I., Turco, E., Zachariasse, W.J., 2005. Long-period orbital control on middle Miocene global cooling: Integrated stratigraphy and astronomical tuning of the Blue Clay Formation on Malta. Paleoceanography 20 (4).

Akers, W.H., 1955. Some planktonic foraminifers of the American gulf coast and suggested correlations with the Caribbean Tertiary. J. Paleontol. 29 (4), 647–664.

Andreyeva-Grigorovich, A.S., Kulchytsky, Y.O., Gruzman, A.D., Lozynyak, P.Y., Petrashkevich, M.I., Portnyagina, L.O., Ivanina, A.V., Smirnov, S.E., Trofimovich, N.A., Savitskaya, N.A., Shvareva, N.J., 1997. Regional stratigraphic scheme of Neogene formations of the Central Paratethys in the Ukraine. Geol. Carpath. 48 (2), 123–136.

Andreyeva-Grigorovich, A.S., Oszczypko, N., Savitskaya, N.A., Ślączka, A., Trofimovich, N.A., 2003. Correlation of Late Badenian salts of the Wieliczka, Bochnia and Kalush areas (Polish and Ukrainian Carpathian Foredeep). Ann. Soc. Geol. Pol. 73, 67–89.

BąBel, M., 1999. History of sedimentation of the Nida Gypsum deposits (Middle Miocene, Carpathian Foredeep, southern Poland). Kwartalnik Geologiczny 43 (4), 429–447.

Báldi, K., Velledits, F., Ćorić, S., Lemberkovics, V., Lőrincz, K., Shevelev, M., 2017. Discovery of the Badenian evaporites inside the Carpathian Arc. implications for global climate change and Paratethys salinity. Geol. Carpath. 68, 193–206.

Bartol, M., Mikuž, V., Horvat, A., 2014. Palaeontological evidence of communication between the Central Paratethys and the Mediterranean in the late Badenian/early Serravalian. Palaeogeogr. Palaeoclimatol. Palaeoecol. 394, 144–157.

Barwicz-Piskorz, W., 1978. The Miocene Radiolaria from the Carpathian Foredeep. Acta Palaeontol. Pol. 23, 223–248.

Barwicz-Piskorz, W., 1997. Badenian (Miocene) radiolaria from the Gliwice area (Upper Silesia, Poland). Bulletin of the Polish Academy of Sciences. Earth Sci. 45 (2–4), 87–95.

Berggren, W.A., Kent, D.V., Swisher Iii, C.C., Aubry, M.P., 1995. A revised Cenozoic geochronology and chronostratigraphy. In: Geochronology, Time Scales and Global Stratigraphic Correlation, pp. 129–212.

Bicchi, E., Ferrero, E., Gonera, M., 2003. Palaeoclimatic interpretation based on Middle Miocene planktonic foraminifera: The Silesia Basin (Paratethys) and Monferrato (Tethys) records. Palaeogeogr. Palaeoclimatol. Palaeoecol. 196, 265–303.

Blow, W.H., 1956. Origin and evolution of the foraminiferal genus Orbulina d'Orbigny. Micropaleontology 2 (1), 57–70.

Bramlette, M.N., Wilcoxon, J.A., 1967. Middle Tertiary calcareous nannoplankton of the Cipero section. In: Trinidad, W.I. (Ed.), Tulane Studies in Geology and Paleontology. 5. pp. 93–131.

Brestenská, E., Jiříček, R., 1978. Ostrakoden des Badenien der Zentralen Paratethys. In: Seneš, J. (Ed.), Chronostratigraphie und Neostratotypen: M4 Badenien. Verlag der Slowakischen Akademie der Wissenschaften, Bratislava, pp. 405–439.

Brönnimann, P., 1951. The genus Orbulina d'Orbigny in the Oligo-Miocene. In: Trinidad, B.W.I. (Ed.), Contributions from the Cushman Foundation for Foraminiferal Research. Vol. 2. pp. 132–138.

Brönnimann, P., Stradner, H., 1960. Die Foraminiferen- und Discoasteriden-zonen von Kuba und ihre interkontinentale Korrelation. Erdoel-Zeitschrift 76 (10), 364–369.

Browning, J.V., Miller, K.G., Sugarman, P.J., Kominz, M.A., McLaughlin, P.P., Kulpecz, A.A., Feigenson, M.D., 2008. 100 Myr record of sequences, sedimentary facies and sea level change from Ocean Drilling Program onshore coreholes, US Mid-Atlantic coastal plain. Basin Res. 20 (2), 227–248.

Bukowski, K., de Leeuw, A., Gonera, M., Kuiper, K.F., Krzywiec, P., Peryt, D., 2010. Badenian tuffite levels within the Carpathian orogenic front (Gdów-Bochnia area, Southern Poland): Radio-isotopic dating and strati graphic position. Geological Quarterly 54 (4), 449–464.

Bukry, D., 1971. Cenozoic calcareous nannofossils from the Pacific Ocean. San Diego Society of Natural History Transactions 16, 303–327.

Bukry, D., Bramlette, M.N., 1969. Some new and stratigraphically useful calcareous nannofossils of the Cenozoic. Tulane Studies in Geology 7, 131–142.

Cernajsek, T., 1974. Die Ostracodenfaunen der Sarmatischen Schichten in Österreich. In: Papp, A., Marinescu, F., Seneš, J. (Eds.), M5 Sarmatien, Die Sarmatische Schichtengruppe und ihr Stratotypus. Chronostratigraphie und Neostratotypen, Miozän der Zentralen Paratethys. Veda Verlag Slowak. Akad. Wiss, Bratislava, pp. 458–491.

Chira, C., 2000. Nannoplancton Calcaros si moluste Miocene din Transilvania. Carpatica Cluj-Napoca, Romania (183 pp).

Cicha, I., Rögl, F., Rupp, C., Ctyroká, J., 1998. Oligocene –Miocene foraminifera of the Central Paratethys. Abhandlungen der Senckenbergischen Naturforschenden Gesellschaft 549, 1–325.

CIESM, 2008. The Messinian salinity crisis from mega-deposits to microbiology – A consensus report. In: Briand, F. (Ed.), N33 in CIESM Workshop Monographs. Monaco, pp. 168.

Crihan, I.M., 1999. Palaeocology of the Badenian Foraminifera bethween the Prahova Valley and Teleajen Valley (Subcarpathians of Muntenia). Geol. Carpathica 52.

Cushman, J.A., 1918. Some Miocene foraminifers of the coastal plain of the United States. U.S. Geol. Surv. Bull. 676.

Cushman, J.A., Jarvis, P.W., 1936. Three new foraminifera from the Miocene Bowden marl of Jamaica. Contr. Cushman Found. Foraminiferal Res. 12 (1), 3–5.

de Boer, B., Van De Wal, R.S.W., Bintanja, R., Lourens, L.J., Tuenter, E., 2010. Cenozoic global ice-volume and temperature simulations with 1-D ice-sheet models forced by benthic δ18O records. Ann. Glaciol. 51 (55), 23–33.

de Leeuw, A., Bukowski, K., Krijgsman, W., Kuiper, K.F., 2010. Age of the Badenian Salinity Crisis; Impact of Miocene climate variability on the circum-mediterranean region. Geology 38 (8), 715–718.

de Leeuw, A., Filipescu, S., Maţenco, L., Krijgsman, W., Kuiper, K., Stoica, M., 2013. Paleomagnetic and chronostratigraphic constraints on the Middle to Late Miocene evolution of the Transylvanian Basin (Romania): Implications for Central Paratethys stratigraphy and emplacement of the Tisza–Dacia plate. Glob. Planet. Chang. 103, 82–98.

Deflandre, G., 1947. Braarudosphaera nov. gen., type d'une famille nouvelle de Coccolithophorides actuels a elements composites. In: Comptes Rendus Hebdomadaires des Séances. Vol. 225. de l'Académie des Sciences, Paris, pp. 439–441.

Deflandre, G., 1953. Hétérogénéité intrinsèque et pluralité des éleménts dans les coccolithes actuels et fossiles. Vol. 237. Comptes Rendus (Hebdomadaires des Séances) de l'Académie des Sciences, Paris, pp. 1785–1787.

D'Orbigny, A.D., 1826. Tableau méthodique de la classe des céphalopodes. Ann. Sci. Nat. Paris, Ser. 1 (7), 96–314.

Dumitrică, P., 1978. Badenian radiolaria from central paratethys. In: Brestenska, E. (Ed.), Chronostratigraphie and Neostratotypen. Miozän der Zentralen Paratethys. Miozän M4-Badenien. VEDA, Bratislava, pp. 231–261.

Filipescu, S., 2001. Wielician foraminifera at the western border of the Transylvanian Basin. Stud. Univ. Babes-Bolyai, Geol. XLVI (2), 115–123.

Filipescu, R., Filipescu, S., 2015. New data on the Early - Middle Badenian transition in the NW Transylvanian Basin (Romania) revealed by the planktonic foraminifera assemblages. Studia UBB Geologia, 2014-2015 59 (1-2), 39–44.

Frunzescu, D., 2005. A sedimentological analysis of the sulphatic evaporitic lithofacies in the salt breccia in Valea Rea, Istrita Hill (Carpathians Foredeep). Annual of the University of Mining and Geology St. Ivan Rilski 48 (1), 81–90.

Frunzescu, D., 2010. Types of lithological sequences and successions in the tuff and gypsum subformations of Low Badenian from Piatra Verde (Slănic-Teişani). In: Proceedings of the XIX CBGA Congress. Scientific Annals. School of Geology, Aristotle University of Thessaloniki, Thessaloniki, pp. 449–456 Special Volume 99.

Frunzescu, D., 2012. Miocene evaporites from the southern part of Eastern Carpathians – sedimentological approach. Romanian J. Min. Depos. 85 (2), 22–29.

Frunzescu, D., Crihan, I.M., Cehlarov, A., Brănoiu, G., 2010. Sedimentological study of the Lower Sarmatian gypsums from Salcia. Prahova district In: Annual Conference of the Geological Society of Romania, Bucharest, pp. 53–58.

Garecka, M., Olszewska, B., 2011. Correlation of the middle Miocene deposits in se Poland and Western Ukraine based on foraminifera and calcareous nannoplankton. Ann. Soc. Geol. Pol. 81 (3), 309–330.

Gonera, M., 2013. Globorotaliid intervals of the sub-evaporite Badenian (Middle Miocene) in the Upper Silesia Basin (Central Paratethys, Poland). Geol. Quart. 57 (4).

Gonera, M., Peryt, T.M., Durakiewicz, T., 2000. Biostratigraphic and palaeoenvironmental implications of isotopic studies (^{18}O, ^{13}C) of Middle Miocene (Badenian) foraminifers in the Central Paratethys. Terra Nova 12, 231–238.

Gradstein, F.M., Ogg, J.G., Schmitz, M.D., Ogg, G.M., 2012. The Geologic Time Scale 2012. Geol. Time Scale (1–2), 1–1144.

Gran, H.H., Braarud, T., 1935. A quantitative study of the phytoplankton in the Bay of Fundy and the Gulf of Maine (including observations on hydrography, chemistry and turbidity). J. Biol. Board Canada 1, 279–467.

Gross, M., 2006. Middle Miocene Ostracods from the Vienna Basin (Badenian/Sarmatian, Austria). Verlag der Österreichischen Akademie der. Wissenschaften, Wien, pp. 226.

Harzhauser, M., Piller, W.E., 2007. Benchmark data of a changing sea - Palaeogeography, Palaeobiogeography and events in the Central Paratethys during the Miocene. Palaeogeogr. Palaeoclimatol. Palaeoecol. 253 (1–2), 8–31.

Harzhauser, M., Peckmann, J., Birgel, D., Draganits, E., Mandic, O., Theobalt, D., Huemer, J., 2014. Stromatolites in the Paratethys Sea during the Middle Miocene climate transition as witness of the Badenian Salinity Crisis. Facies 60 (2), 429–444.

Hay, W.W., Mohler, H.P., Roth, P.H., Schmidt, R.R., Boudreaux, J.E., 1967. Calcareous nannoplankton zonation of the Cenozoic of the Gulf Coast and Caribbean-Antillean area, and transoceanic correlation. Trans. Gulf Coast Assoc. Geol. Soc. 17, 428–480.

Hilgen, F.J., Krijgsman, W., Raffi, I., Turco, E., Zachariasse, W.J., 2000. Integrated stratigraphy and astronomical calibration of the Serravallian/Tortonian boundary section at Monte Gibliscemi (Sicily, Italy). Mar. Micropaleontol. 38 (3–4), 181–211.

Hilgen, F.J., Abdul Aziz, H., Krijgsman, W., Raffi, I., Turco, E., 2003. Integrated stratigraphy and astronomical tuning of the Serravallian and lower Tortonian at Monte dei Corvi (Middle-Upper Miocene, northern Italy). Palaeogeogr. Palaeoclimatol. Palaeoecol. 199 (3–4), 229–264.

Hilgen, F.J., Abels, H.A., Iaccarino, S., Krijgsman, W., Raffi, I., Sprovieri, R., Turco, E., Zachariasse, W.J., 2009. The Global stratotype section and point (GSSP) of the Serravallian stage (Middle Miocene). Episodes 32 (3), 152–166.

Hilgen, F.J., Lourens, L.J., van Dam, J.A., 2012. The neogene period. In: Gradstein, F.M., Ogg, J.G., Schmitz, M., Ogg, G. (Eds.), The Geologic Time Scale 2012. Elsevier Science, pp. 923–978.

Hodell, D.A., Curtis, J.H., Sierro, F.J., Raymo, M.E., 2001. Correlation of late Miocene to early Pliocene sequences between the Mediterranean and North Atlantic. Paleoceanography 16 (2), 164–178.

Hohenegger, J., Coric, S., Wagreich, M., 2014. Timing of the Middle Miocene Badenian Stage of the Central Paratethys. Geol. Carpath. 65 (1), 55–66.

Holbourn, A., Kuhnt, W., Schulz, M., Flores, J.A., Andersen, N., 2007. Orbitally-paced climate evolution during the middle Miocene "Monterey" carbon-isotope excursion.

Earth Planet. Sci. Lett. 261 (3–4), 534–550.
Kamp, P.J.J., Vonk, A.J., Bland, K.J., Hansen, R.J., Hendy, A.J.W., McIntyre, A.P., Ngatai, M., Cartwright, S.J., Hayton, S., Nelson, C.S., 2004. Neogene stratigraphic architecture and tectonic evolution of Wanganui, King Country, and eastern Taranaki Basins, New Zealand. N. Z. J. Geol. Geophys. 47 (4), 625–644.
Kamptner, E., 1954. Untersuchungen über den Feinbau der Coccolithen. Arch. Protistenkd. 100, 1–90.
Kamptner, E., 1963. Coccolithineen-Skelettreste aus Tiefseeablagerungen des Pazifischen Ozeans. Annalen des Naturhistorischen Museums in Wien 66, 139–204.
Karami, M.P., de Leeuw, A., Krijgsman, W., Meijer, P.T., Wortel, M.J.R., 2011. The role of gateways in the evolution of temperature and salinity of semi-enclosed basins: An oceanic box model for the Miocene Mediterranean Sea and Paratethys. Glob. Planet. Chang. 79 (1–2), 73–88.
Koppers, A.A.P., 2002. ArArCALC-software for $^{40}Ar/^{39}Ar$ age calculations. Comput. Geosci. 28 (5), 605–619.
Kováč, M., Kováč, P., Marko, F., Karoli, S., Janočko, J., 1995. The East Slovakian Basin – a complex back-arc basin. Tectonophysics 252, 453–466.
Kováč, M., Hudáčková, N., Rudinec, R., Lankreijer, A., 1996. Basin evolution in the foreland and hinterland of the Carpathian accretionary prism during the Neogene: evidence from the Western to Eastern Carpathians Junction. Ann. Tectonicae, Firenze 1–2, 3–19.
Kováč, M., Andreyeva-Grigorovich, A., Bajraktarević, Z., Brzobohatý, R., Filipescu, S., Fodor, L., Harzhauser, M., Nagymarosy, A., Oszczypko, N., Pavelić, D., Rögl, F., Saftić, B., Sliva, L., Studencka, B., 2007. Badenian evolution of the Central Paratethys Sea: Paleogeography, climate and eustatic sea-level changes. Geol. Carpath. 58 (6), 579–606.
Krézsek, Cs., Filipescu, S., 2005. Middle to Late Miocene sequence stratigraphy of the Transylvanian Basin (Romania). Tectonophysics 410 (1–4), 437–463.
Krijgsman, W., Garcés, M., Agustí, J., Raffi, I., Taberner, C., Zachariasse, W.J., 2000. The 'Tortonian salinity crisis' of the eastern Betics (Spain). Earth Planet. Sci. Lett. 181 (4), 497–511.
Krijgsman, W., Gaboardi, S., Hilgen, F.J., Iaccarino, S., de Kaenel, E., Van der Laan, E., 2004. Revised astrochronology for the Ain el Beida section (Atlantic Morocco): No glacio-eustatic control for the onset of the. Messinian Salinity Crisis Stratigr. 1, 87–101.
Krijgsman, W., Stoica, M., Vasiliev, I., Popov, V.V., 2010. Rise and fall of the Paratethys Sea during the Messinian Salinity Crisis. Earth Planet. Sci. Lett. 290 (1–2), 183–191.
Kuiper, K.F., Deino, A., Hilgen, F.J., Krijgsman, W., Renne, P.R., Wijbrans, J.R., 2008. Synchronizing rock clocks of earth history. Science 320 (5875), 500–504.
Lanphere, M.A., Dalrymple, G.B., Fleck, R.J., Pringle, M.S., 1990. Intercalibration of mineral standards for K–Ar and $^{40}Ar/^{39}Ar$ age measurements (abstract). Trans. Am. Geophys. Union 71, 1658.
Leroy, L.W., 1939. Some small foraminifera, Ostracoda and otoliths from the Neogene ("Miocene") of the Rokan-Tapanoeli area, central Sumatra. Natuurk. Tijdschr. Nederl.-Indie 99 (6), 215–296.
Loeblich Jr., A.R., Tappan, H., 1978. The Coccolithophorid Genus Calsidiscus Kamptner and its Synonyms. J. Paleontol. 52 (6), 1390–1392.
Martini, E., 1971. Standard Tertiary and Quaternary calcareous nannoplankton zonation. In: Farinacci, A. (Ed.), Proceedings of the Second International Conference on Planktonic, Microfossils. Ed. Tecnosci, Roma, pp. 739–785.
Martini, E., Bramlette, M.N., 1963. Calcareous nannoplankton from the experimental Mohole drilling. J. Paleontol. 37, 845–855.
Mărunţeanu, M., 1999. Litho- and biostratigraphy (calcareous nannoplankton) of the Miocene deposits from the Outer Moldavides. Geol. Carpath. 50 (4), 313–324.
Matenco, L., Bertotti, G., Cloetingh, S., Dinu, D., 2003. Subsidence analysis and tectonic evolution of the external Carpathian–Moesian Platform region during Neogene times. Sediment. Geol. 156, 71–94.
McDougall, I., Harrison, T.M., 1999. Geochronology and Thermochronology by the $^{40}Ar/^{39}Ar$ Method. Oxford Univerity Press.
Melinte-Dobrinescu, M.C., Stoica, M., 2014. Badenian calcareous nannofossil fluctuation in the Eastern Carpathians: Palaeoenvironmental significance. Acta Palaeontol. Romaniae 9 (2), 47–57.
Miller, K.G., Kominz, M.A., Browning, J.V., Wright, J.D., Mountain, G.S., Katz, M.E., Sugarman, P.J., Cramer, B.S., Christie-Blick, N., Pekar, S.F., 2005. The phanerozoic record of global sea-level change. Science 310 (5752), 1293–1298.
Min, K., Mundil, R., Renne, P.R., Ludwig, K.R., 2000. A test for systematic errors in 40Ar/39Ar geochronology through comparison with U/Pb analysis of a 1.1-Ga rhyolite. Geochim. Cosmochim. Acta 64, 73–98.
Morgan, L.E., Renne, P.R., Taylor, R.E., Woldegabriel, G., 2009. Archaeological age constraints from extrusion ages of obsidian: Examples from the Middle Awash, Ethiopia. Quat. Geochronol. 4 (3), 193–203.
Motaş, I., Bandrabur, T., Ghenea, C., Săndulescu, M., 1966. Geologic map of Romania; 1:200,000. (Ploiesti sheet).
Mullender, T.A.T., Van Velzen, A.J., Dekkers, M.J., 1993. Continuous drift correction and separate identification of ferrimagnetic and paramagnetic contributions in thermomagnetic runs. Geophys. J. Int. 114 (3), 663–672.
Münster, G., 1830. Über einige fossile Arten Cypris (Müller, Lamk.) und Cythere (Müller, Latreille, Desmarest). Jahrbuch für Mineralogie, Geognosie. Geologie und Petrefaktenkunde 1, 60–67.
Murgeanu, G., Patrulius, D., Gherasi, N., Ghenea, C., 1967. Geologic map of Romania; 1:200,000. (Targoviste sheet).
Murray, G., Blackman, V.H., 1898. On the nature of the coccospheres and rhabdospheres. Philos. Trans. Royal Soc. Lond. (B) 190 (1), 427–441.
Nejbert, K., Śliwiński, M.G., Benowitz, J., Layer, P., Yatsyshyn, A., Tomeniuk, O., Olszewska-Nejbert, D., Bąbel, M., 2012. 40Ar/39Ar dating of late Badenian pyroclastic deposits from Schyrets'(near Lviv, Ukraine) and its stratigraphic significance. In: Józsa, Š., Reháková, D., Vojtko, R. (Eds.), Structural and Stratigraphical Evolution of the Western Carpathians 8th Conference 2012. Abstract Book, Bratislava, pp. 33.
Nier, A.O., 1950. A redetermination of the relative abundances of theisotopes of carbon, nitrogen, oxygen, argon, and potassium. Phys. Rev. 77, 789–793.
Osmólski, T., 1972. The influence of the geological structure of marginal parts of the Działoszyce Trough on the metasomatosis of gypsum. Biuletyn Instytutu Geologicznego 260, 65–188.
Palcu, D.V., Tulbure, M., Bartol, M., Kouwenhoven, T.J., Krijgsman, W., 2015. The Badenian–Sarmatian Extinction Event in the Carpathian foredeep basin of Romania: Paleogeographic changes in the Paratethys domain. Glob. Planet. Chang. 133, 346–358.
Palcu, D.V., Golovina, L.A., Vernyhorova, Y.V., Popov, S.V., Krijgsman, W., 2017. Middle Miocene paleoenvironmental crises in Central Eurasia caused by changes in marine gateway configuration. Glob. Planet. Chang. 158, 57–71.
Palotai, M., Csontos, L., 2012. Flexural basin reworked by salt-related pull-apart structures: The Adony Basin. Central Eur. Geol. 55 (2), 147–180.
Papp, A., Cicha, I., Seneš, J., Steininger, F. (Eds.), 1978. Chronostratigraphie und Neostratotypen. M4 Badenien, Miozän der Zentralen Paratethys. VEDA, Bratislava, pp. 1–593.
Perch-Nielsen, K., 1984. Validation of new combinations. INA Newsletter 6 part 2, 42–46.
Peryt, D., 1997. Calcareous nannoplankton stratigraphy of the Middle Miocene in the Gliwice area (Upper Silesia, Poland). Bull. Pol. Acad. Sci. Earth Sci. 45, 119–131.
Peryt, D., 1999. Calcareous nannoplankton assemblages of the Badenian evaporites in the Carpathian Foredeep. Biul. Państw. Inst. Geol. 387, 158–161.
Peryt, T.M., 2006. The beginning, development and termination of the Middle Miocene Badenian Salinity Crisis in Central Paratethys. Sediment. Geol. 188-189, 379–396.
Peryt, D., 2013a. Foraminiferal record of marine transgression during deposition of the Middle Miocene Badenian evaporites in Central Paratethys (Borków section, Polish Carpathian Foredeep). Terra Nova 25 (4), 298–306.
Peryt, D., 2013b. Foraminiferal record of the Middle Miocene climate transition prior to the Badenian Salinity Crisis in the Polish Carpathian Foredeep Basin (Central Paratethys). Geol. Quart. 57 (1), 141–164.
Peryt, D., Peryt, T., 2009. Environmental changes in the declining Middle Miocene Badenian evaporite basin of the Ukrainian Carpathian Foredeep (Kudryntsi section). Geol. Carpath. 60 (6), 505–517.
Peryt, T.M., Durakiewicz, T., Peryt, D., Poberezhskyy, A., 2012. Carbon and oxygen isotopic composition of the middle Miocene Badenian gypsum-associated limestones of West Ukraine. Geol. Acta 10 (4), 319–332.
Peryt, D., Gedl, P., Peryt, T.M., 2014. Foraminiferal and palynological records of the Late Badenian (Middle Miocene) transgression in Podolia (Shchyrets near Lviv, western Ukraine). Geol. Quart. 58 (3), 465–484.
Piller, W.E., Harzhauser, M., Mandic, O., 2007. Miocene Central Paratethys stratigraphy – current status and future directions. Stratigraphy 4 (2/3), 151–168.
Popescu, G., 1951. Observaţii asupra breciei sării şi a unor masive de sare din regiunea paleogen - miocenă a judeţului Prahova. Dări de Seamă ale Institutului Geologic 32, 3–13.
Popescu, G., 1970. Planktonic foraminiferal zonation in the Dej Tuff complex. Revue Roumanie de Geologie. Geophysique et Geographie, Serie de Geologie 14 (2), 189–203.
Popescu, G., 1987. Marine Middle Miocene microbiostratigraphical correlation in Central Paratethys. Dari de Seama ale Institutului de Geoogie si Geofizica 72–73 (3), 149–167.
Popescu, G., Crihan, I.M., 2004. Contributions to the knowledge of the Miocene foraminifera from Romania: superfamily Nodosariacea (fam. Nodosariidae and Vaginulinidae). Acta Palaeontol. Romaniae 4, 385–402.
Popescu, G., Crihan, I.M., 2011. Middle Miocene Globigerinas of Romania. Acta Palaeontol. Romaniae 7, 291–314.
Popov, S.V., Rögl, F., Rozanov, A.Y., Steininger, F.F., Shcherba, I.G., Kováč, M., 2004. Lithological-Paleogeographic maps of Paratethys, 250: Frankfurt, Cour. Forsch.-Inst. Senckenberg 46.
Procházka, V.J., 1893. Miocaen Židlochovický na Moravě a jeho zvířena (Das Miocaen von Seelowitz in Moravia und dessen Fauna). Rozpravy České Akad 2 (24), 1–90.
Raffi, I., Backman, J., Fornaciari, E., Pälike, H., Rio, D., Lourens, L., Hilgen, F., 2006. A review of calcareous nannofossil astrobiochronology encompassing the past 25 million years. Quat. Sci. Rev. 25 (23–24), 3113–3137.
Renne, P.R., Swisher, C.C., Deino, A.L., Karner, D.B., Owens, T.L., Depaolo, D.J., 1998. Intercalibration of standards, absolute ages and uncertainties in 40Ar/ 39Ar dating. Chem. Geol. 145 (1–2), 117–152.
Reuss, A.E., 1850a. Die fossilen Entomostraceen des österreichischen Tertiärbeckens. Haidingers naturwiss 3 (1), 41–92.
Reuss, A.E., 1850b. Neues Foraminiferen aus den Schichten des osterreichischen Tertiarbeckens. Math.-Naturw 1, 365–390.
Rögl, F., 1998. Palaeogeographic considerations for Mediterranean and Paratethys seaways (Oligocene to Miocene). Annalen des Naturhistorischen Museums Wien 99, 279–310.
Roveri, M., Flecker, R., Krijgsman, W., Lofi, J., Lugli, S., Manzi, V., Sierro, F.J., Bertini, A., Camerlenghi, A., De Lange, G., Govers, R., Hilgen, F.J., Hübscher, C., Meijer, P.T., Stoica, M., 2014. The Messinian salinity crisis: Past and future of a great challenge for marine sciences. Mar. Geol. 352, 25–58.
Ruggieri, G., Sprovieri, R., 1970. I microforaminiferi delle marne di S. Cipirello. Lavori Ist. Geol. Palermo 10, 1–26.
Săndulescu, M., 1984. Geotectonica Romaniei (Geotectonics of Romania). Ed. Tehnica, Bucharest, pp. 450 pp. (in Romanian).
Sant, K., de Leeuw, A., Chang, L., Czapowski, G., Gąsiewicz, A., Krijgsman, W., 2015. Paleomagnetic analyses on Badenian-Sarmatian drill cores from the North Carpathian Foredeep (Middle Miocene, Poland). Bull. Polish Geol. Ins. 461, 179–192.

Scarponi, D., Bella, G.D., Dell'Angelo, B., Huntley, J.W., Sosso, M., 2016. Middle Miocene Conoidean Gastropods from Western Ukraine (Paratethys): Integrative Taxonomy, Palaeoclimatogical and Palaeobiogeographical Implications. Acta Palaeontol. Pol. 61 (2), 327–344.
Schiller, J., 1930. Coccolithinae. In: Rabenhorst, L. (Ed.), Kryptogamenflora. 10. Akademische Verlagsgessellschaft, pp. 89–273.
Schleder, Z., Man, S., Tamas, D., 2016. History of salt tectonics in the Carpathian bend zone. In: Romania - Guide for the Pre-Conference Field Trip, Bucharest, pp. 22.
Śliwiński, M., Bábel, M., Nejbert, K., Olszewska-Nejbert, D., Gásiewicz, A., Schreiber, B.C., Benowitz, J.A., Layer, P., 2012. Badenian-Sarmatian chronostratigraphy in the Polish Carpathian Foredeep. Palaeogeogr. Palaeoclimatol. Palaeoecol. 326–328, 12–29.
Ștefănescu, M., Rădan, S., Micu, M., Mărunțeanu, M., Ștefănescu, M., 1978. Geological Map 1:50.000 - Sheet 129b Slanic (Prahova). Printing House of the Romanian Geological and Geophysical institute (IGR), Bucharest.
Steiger, R.H., Jäger, E., 1977. Subcommission on geochronology: Convention on the use of decay constants in geo- and cosmochronology. Earth Planet. Sci. Lett. 36 (3), 359–362.
Steininger, F.F., Rögl, F., 1984. Paleogeography and palinspastic reconstruction of the Neogene of the Mediterranean and Paratethys. Geochem. Soc. Spec. Publ. 659–668.
Stradner, H., Fuchs, R., 1980. Occurrence of nannoplankton in the Sarmatian (upper Miocene) of the central Paratethys in Lower Austria and Burgenland. Beiträge zur Paläontolgie von Österreich 7, 251–279.
Theodoridis, S., 1984. Calcareous nannofossil biostratigraphy of the Miocene and revision of the helicoliths and discoasters. Utrecht Micropaleontol. Bull. 32, 1–271.
Vasiliev, I., Dekkers, M.J., Krijgsman, W., Franke, C., Langereis, C.G., Mullender, T.A.T., 2007. Early diagenetic greigite as a recorder of the palaeomagnetic signal in Miocene-Pliocene sedimentary rocks of the Carpathian foredeep (Romania). Geophys. J. Int. 171 (2), 613–629.
Vasiliev, I., de Leeuw, A., Filipescu, S., Krijgsman, W., Kuiper, K., Stoica, M., Briceag, A., 2010. The age of the Sarmatian-Pannonian transition in the Transylvanian Basin (Central Paratethys). Palaeogeogr. Palaeoclimatol. Palaeoecol. 297 (1), 54–69.
Vasiliev, I., Iosifidi, A.G., Khramov, A.N., Krijgsman, W., Kuiper, K., Langereis, C.G., Popov, V.V., Stoica, M., Tomsha, V.A., Yudin, S.V., 2011. Magnetostratigraphy and radio-isotope dating of upper Miocene-lower Pliocene sedimentary successions of the Black Sea Basin (Taman Peninsula, Russia). Palaeogeogr. Palaeoclimatol. Palaeoecol. 310 (3–4), 163–175.
Venglinskij, I.V., 1975. Foraminifers and biostratigraphy of the Miocene deposits of Transcarpathian Basin. Nauk. Dumka, Kiev 1–264 (in Russian).
Wallich, G.C., 1877. Observations on the coccosphere. Ann. Mag. Nat. Hist. 19, 342–350.
Zachariasse, W.J., Sudijono, W., 2012. New data on the morphology and classification of the oligocene-miocene planktonic foraminifer Paragloborotalia siakensis (Leroy, 1939). J. Foraminifer. Res. 42 (2), 156–168.